

Rapid 3-D Laser Microprinting of Bioscaffolds and Patterning of Proteins

by

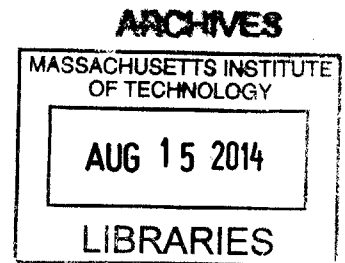
Man-Chi Liu

B.S., Mechanical Engineering
National Taiwan University, 2011

Submitted to the Department of Mechanical Engineering
in Partial Fulfillment of the Requirements for the Degree of

MASTER OF SCIENCE IN MECHANICAL ENGINEERING
at the
MASSACHUSETTS INSTITUTE OF TECHNOLOGY

June 2014



©2014 Massachusetts Institute of Technology. All rights reserved.

Signature redacted

Signature of Author: _____
Department of Mechanical Engineering
May 19, 2014

Signature redacted

Certified by: _____
Mehmet Fatih Yanik
Professor of Electrical Engineering and Computer Science
Thesis Supervisor

Signature redacted

Certified by: _____
Peter T. C. So
Professor of Mechanical Engineering
Mechanical Engineering Thesis Reader

Signature redacted

Accepted by: _____
David E. Hardt
Professor of Mechanical Engineering
Chairman, Committee on Graduate Students

Rapid 3-D Laser Microprinting of Bioscaffolds and Patterning of Proteins

by
Man-Chi Liu

Submitted to the Department of Mechanical Engineering
on May 19, 2014 in Partial Fulfillment of the Requirements for the
Degree of Master of Science in Mechanical Engineering

ABSTRACT

Tissue engineers have been developing biological substitutes to regenerate or replace damaged tissue. Tissues contain both exquisite microarchitectures and chemical cues to support cell migration, proliferation and differentiation. The majority of tissue engineering strategies use porous scaffolds containing chemical cues for culturing cells. However, these methods are unable to truly recapitulate the complexity of the in-vivo environment, limiting the effective regeneration. Several techniques have been developed to create three-dimensional patterns of proteins and 3-D print the architectures of bio-scaffolds for studying and directing cell development. Scott has developed a rapid 3-D laser microprinting system¹, which is able to simultaneously print the defined architecture of scaffolds and internal patterns of proteins inside scaffolds with high-speed and high-resolution.

The object of this thesis is to further develop the technique of rapid 3-D laser microprinting by researching on the biological activity and functions of printed scaffolds and printed proteins. First, we constructed branched collagen microchannels containing microprinted patterns of P-selectin, a protein involved in leukocyte recruitment from blood vessels. We showed that leukocyte rolling occurred on P-selectin patterned collagen channels. Second, we presented a 3-D printed microvasculature by seeding endothelial cells into a printed collagen scaffold with capillary-like microarchitecture. Next, we performed leukocyte rolling assay within the printed microvasculature by printing the patterns of protein cues to activate the endothelium. Last, we created a 3-D microprinted collagen scaffolds for guiding and homing of cells. Cells were guided by printed P-selectin patterns and trapped in specific locations inside collagen scaffolds.

All the work demonstrated that printed protein cues retain their biological activity, and the combination of printed scaffolds and patterned protein cues provides potential application for drug screening assays in biomimetic environments and cell delivery for regenerative medicine. We believe that this rapid printing technology will enable highly engineered therapeutic scaffolds for regenerative medicine applications.

Thesis Supervisor:

Mehmet Fatih Yanik, Professor of Electrical Engineering and Computer Science

Mechanical Engineering Thesis Reader:

Peter T. C. So, Professor of Mechanical Engineering

Abstract	3
Chapter 1: Introduction and Background	7
1.1 3-D printing of scaffolds and patterning of proteins in regenerative medicine	7
1.1.1 Scaffolds for tissue engineering	7
1.1.2 Microarchitecture of scaffolds and patterning of proteins inside scaffolds enables specific cell behavior	8
1.1.3 Existing multi-photon photolithography is promising for generating 3-D microarchitecture of scaffolds and patterns of proteins inside scaffolds	9
1.2 Review of the rapid 3-D laser microprinting technique	10
1.2.1 Photobleaching of biotin-4-fluorescein enables 3-D patterning of proteins	10
1.2.2 Femtosecond laser 3-D microprinting system	11
1.2.3 Schematic for printing biotinylated proteins in scaffold materials	12
1.2.4 Patterns of streptavidin formed in scaffold materials	14
1.2.5 3-D Printing of Collagen Scaffolds by Photobleaching of Fluorescein	15
1.2.6 Combined Printing of Scaffolds and Internal Protein Cues	17
1.3 Scope of thesis work	18
Chapter 2: 3-D Microprinted Collagen Scaffolds Containing Internal P-selectin Patterns for Leukocyte Rolling Assay	20
2.1 Background and Motivation	20
2.1.1 Leukocyte recruitment occurring to the vascular wall	20
2.1.2 Selectins are the main roles in leukocyte rolling	21
2.1.3 Use the rapid 3-D laser microprinting technique to create an in-vitro leukocyte rolling system	22
2.2 Results	23
2.2.1 Schematic for leukocyte rolling system	23
2.2.2 Performance of 3-D leukocyte rolling system	25
2.2.3 HL-60 leukocyte rolling assay	28
2.3 Discussion	29
2.4 Conclusion	31
2.5 Detailed Methods	31
2.5.1 Fabrication of PDMS microfluidic chips	31
2.5.2 Collagen scaffold preparation	32
2.5.3 Printing collagen scaffolds	32
2.5.4 Cell culture	33
2.5.5 Leukocyte rolling assay	33
2.5.6 Image and data analysis	33
Chapter 3: 3-D printed Microvasculature and Leukocyte Rolling Assay	35
3.1 Background and Motivation	35
3.1.1 The role of vascularization in tissue engineering	35
3.1.2 Leukocyte rolling assay within printed microvasculature	36
3.2 Results	37
3.2.1 3-D printed microvasculature	37
3.2.2 Schematic for leukocyte rolling in printed microvasculature	41

3.2.3	Improvement in formation of microvasculature.....	42
3.2.4	HL-60 leukocyte rolling assay within printed microvasculature.....	44
3.3	Discussion	45
3.4	Conclusion.....	46
3.5	Detailed Methods	47
3.5.1	Cell culture	47
3.5.2	Formation of microvasculature.....	47
3.5.3	Staining of microvasculature.....	47
3.5.4	Leukocyte rolling assay	48
3.5.5	Image and data analysis	48
Chapter 4:	Guiding and Homing of Cells in 3-D Microprinted Collagen Scaffolds	49
4.1	Background and Motivation	49
4.1.1	Artificial stem cell niche in regenerative medicine	49
4.1.2	Guiding and homing of cells: the first step to create an artificial stem cell niche using rapid 3-D laser microprinting.....	50
4.2	Results.....	51
4.2.1	Schematic for guiding and homing of cells.....	51
4.2.2	Cycle of innovation.....	54
4.2.3	Design evolution	55
4.3	Discussion	60
4.4	Conclusion.....	61
4.5	Detailed Methods	62
4.5.1	Preparation of 3-D microprinted collagen scaffolds for guiding and homing of cells	62
4.5.2	Experiment for guiding and homing of cells.....	62
4.5.3	Image and data analysis	62
Chapter 5:	Conclusion	63
5.1	Summary and Conclusion	63
5.2	Potential Future Work	65
5.2.1	Improvement of leukocyte rolling assay in printed microvasculature.....	65
5.2.2	Next steps for creating engineered stem cell niche.....	65
Reference	68

Chapter 1: INTRODUCTION AND BACKGROUND

1.1 3-D printing of scaffolds and patterning of proteins in regenerative medicine

1.1.1 Scaffolds for tissue engineering

Regenerative medicine is an evolving field in which scientists and engineers have been developing a variety of tools for restoring, maintaining or improving tissue function or a whole organ, and these tools rely on a wide range of technologies including tissue engineering, gene therapy and stem-cell biology². Cell-based therapy, in which cellular materials are directly injected into the human body, provides a method for replacing or repairing damaged tissue or cells. One of widely used cell-based therapies is haematopoietic stem-cell transplantation, in which radiation or chemotherapy is implemented to destroy all haematopoietic cells in patient's body to cure cancers, and then new haematopoietic stem-cells are transplanted into the blood stream³. Although some cell-based therapies have been demonstrated to provide effective regeneration, the direct injection is not sufficient in most tissue types. Therefore, in tissue engineering, the common strategies for developing an engineered tissue to substitute or repair the injured tissues include living cells, biocompatible materials, biochemical (e.g. growth factors) and physical (e.g. shear flow or cyclic mechanical loading) tissue-inducing factors⁴.

Scaffolds are porous, absorbable synthetic or natural polymer for mimicking the structures of extracellular matrices. Scaffolds not only serve the three-dimensional cell culture environment, but also provide induction for tissue formation or cell differentiation based on the material properties or by containing regulators. Biomaterials served as scaffolds have been studied extensively. Scaffolds can be roughly categorized into two types: decellularized scaffolds and artificial scaffolds. Decellularized scaffolds are obtained from the removal of cells from a tissue or an organ, leaving the complex mixture of structural and functional proteins of extracellular matrix⁵. After perfusing patient-derived stem-cells into the decellularized scaffolds, the recellularized scaffolds are implanted into the patient. The reliance on a donor tissue or organ limits the application of decellularized scaffolds. For artificial scaffolds, a variety of biomaterials

and fabrication techniques have been extensively studied. The artificial scaffolds can also be roughly categorized into synthetic polymers and natural polymers⁶. Synthetic polymers such as polyglycolic acid (PGA), polylactic acid (PLLA), their copolymers (e.g. PLGA) and polycaprolactone (PCL) are the commonly used polymers for artificial scaffolds. The natural polymers used for artificial scaffolds include fibrin, collagen, elastin, gelatin, hyaluronic acid (HA), agarose, chitosan and alginate. The most common method for generating scaffolds is the freeze-dry method, that the porosities of scaffolds can be controlled via temperature. Many other factors are taken into account in scaffold design, such as degradation rate and the stiffness of the scaffolds.

1.1.2 Microarchitecture of scaffolds and patterning of proteins inside scaffolds enables specific cell behavior

The freeze-dry method has been demonstrated to provide isotropic scaffolds. However, in some applications, anisotropy is desired. Many studies indicated that the microarchitecture inside scaffolds enables specific cell behavior. Myocardial cells seeded onto a laser ablated scaffold with an accordion-like architecture have been shown to recapitulate native heart structure better than traditional isotropic scaffolds⁷. 3-D printers have been used to generate blood vessel architectures by printing a sacrificial mold out of carbohydrate glass⁸. In nerve regeneration, the artificial, aligned honeycomb scaffolds have been demonstrated to successfully support neural regeneration⁹⁻¹¹. A variety of microfabrication techniques have been investigated to create such microarchitecture inside scaffolds, such as stereolithography, selective laser sintering, 3-D printing, wax printing, fused deposition modeling and bioplotter¹².

As mentioned in 1.1.1, the biochemical inducing factors are also essential for engineered tissue. The biochemical inducing factors, such as morphogens, growth factors and guidance factors, are the proteins inside extracellular matrix that enables tissue formation. The infusion of growth factors into the scaffolds has been demonstrated to enhance cell proliferation and survival¹³. Many adhesive peptides have been used for promoting the robust cell-adhesion inside engineered scaffolds^{14,15}. While growth factors and adhesive peptides are only used for

homogeneous infusion into scaffolds, producing defined patterns of protein cues inside scaffold could enable the formation of more complex tissue formation, such as stem cell niche.

1.1.3 Existing multi-photon photolithography is promising for generating 3-D microarchitecture of scaffolds and patterns of proteins inside scaffolds

As described in 1.1.2, there are many existing techniques for creating 3-D architectures of scaffolds, while there are relative few techniques for creating 3-D patterns of proteins inside scaffolds. Among existing methods, multi-photon photolithography (MPP) is promising for simultaneously generating 3-D microarchitectures of scaffolds and patterns of proteins inside scaffolds. A scanning infra-red (IR) femtosecond pulsed laser is used to excite a multi-photon photoinitiator at the focal point^{16,17}. By stepping the objective, the focal point can be shifted along z-axis, achieving arbitrary three-dimensional shapes to be printed. However, the existing 3-D multi-photon microfabrication methods are too slow to generate scaffolds on a therapeutic scale. In addition, MPP has never been used to print both the scaffold and internal protein cues simultaneously.

In the PhD thesis of Mark A. Scott at Massachusetts Institute of Technology in 2012¹, he has developed a rapid 3-D laser microprinting technique, which can perform printing of collagen scaffolds and patterning of proteins inside scaffolds simultaneously (Fig 1.1). In the next two sections, we will first review this technique and then discuss the following development from the review.

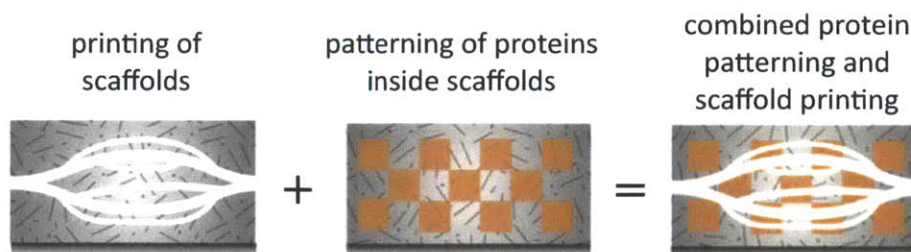


Fig 1.1: Schematic for the rapid 3-D laser microprinting. It combined the printing of scaffolds and the patterning of proteins.

1.2 Review of the rapid 3-D laser microprinting technique

1.2.1 Photobleaching of biotin-4-fluorescein enables 3-D patterning of proteins

Biotin-4-fluorescein (B4F) is a molecule used for all existing protein patterning by photobleaching literature (Fig 1.2). Fluorescein, a fluorophore widely used in microscopy, becomes free radical and binds to a nearby surface upon excitation. Biotin, which is commonly used to conjugate proteins for biochemistry assays, has high affinity (10^{-14} to 10^{-15} M) to the protein streptavidin. Streptavidin is a tetramer, and each of four subunits binds to biotin with the same affinity. Since the four binding sites are arranged as two pairs on opposite sides of streptavidin, we can use them to bind to B4F, while the remaining biotin binding sites on the other sides can be used to pull down other biotinylated proteins. Thus, to generate a protein pattern in three dimensions, we can first perform photobleaching of B4F by multiphoton photolithography method, add streptavidin to bind to B4F, and then add the desired biotinylated protein.

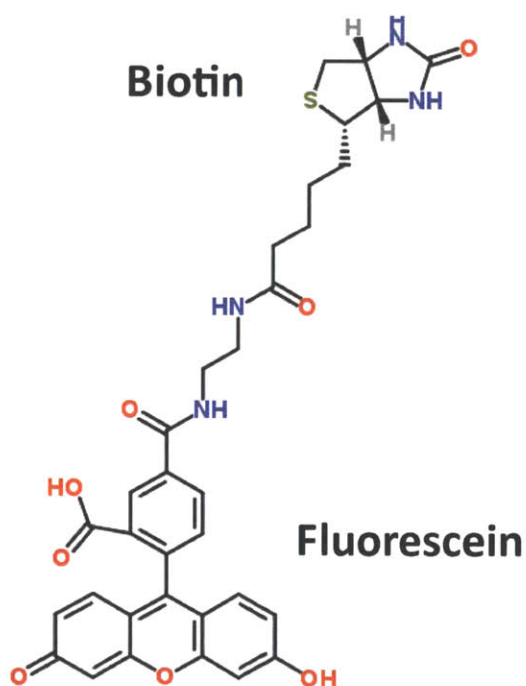


Fig 1.2: Molecular structure of biotin-4-fluorescein. The molecular structure was obtained from the *ChemSpider* database.

1.2.2 Femtosecond laser 3-D microprinting system

Multiphoton photolithography (MPP) has the advantage that the excitation only occurs at the focal spot of the laser, so MPP can be used for printing 3-dimensional patterns. To perform MPP for photobleaching of B4F, a femtosecond laser 3-D microprinting system was assembled as shown in Fig 1.3c.

The data for printing a 3-D object is uploaded to the computer in the form of a series of pictures, with each picture representing a z-section slicing of the 3-D object. These pictures can be obtained from voxel datasets or the 3-D models designed in SolidWorks (Dassault Systèmes SolidWorks Corporation, Waltham, MA). For the 3-D model designed in SolidWorks, the stereolithography (.stl) file is passed to a z-section slicing program, which outputs a series of bitmap pictures of z-sections of the 3-D model (Freesteele Slicer). As shown in Fig 1.3a, the series of pictures is converted into a series of x-, y-, z-coordinates and laser power (i.e. brightness) signals via a custom build MATLAB (MathWorks, Natick, MA) interpreter. This series of signals is then uploaded to NI-DAQ 6259 PCIe card (National Instruments, Austin, TX) for outputting synchronized signals to the femtosecond laser 3-D microprinting system.

In the femtosecond laser 3-D microprinting system, a MAITAI femtosecond laser (Newport) is tuned to 780 nm, performing the two-photon excitation for photobleaching of B4F. The laser power is modulated via an EOM (Newport Corporation, Irvine, CA). A pair of galvanometer scan mirrors (Cambridge Technologies, Cambridge, MA) controls x and y scanning. The laser is focused by a 40X NA objective mounted on a z-axis piezo actuator (PI, Auburn, MA). The four analog signals from NI-DAQ card transmit to the two scan mirrors for x-y scanning, the piezo for z scanning and the EOM for laser power controlling. The x, y, z and laser power signals are synchronized to perform printing in one section of volume. After a volume has been printed, the stage translates to a new location and patterning resumes (Fig 1.3b).

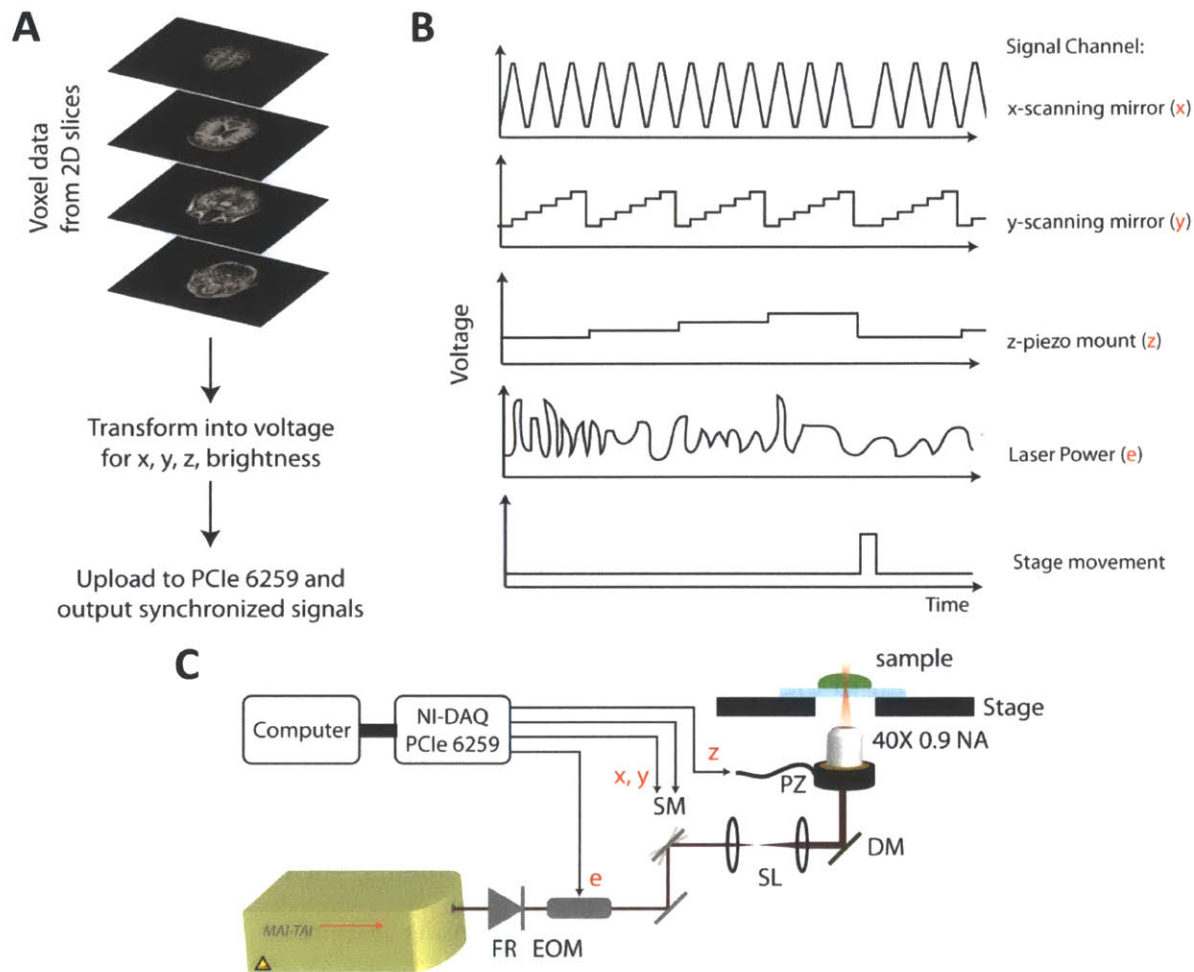


Fig 1.3: A laser setup for rapid 3-D laser microprinting. (a) The data for printing a 3-D object is uploaded to the computer in the form of a series of pictures representing z-slices, which are transformed into voltage signals to be uploaded to the NI-DAQ card. (b) The voltage signals to perform 3-D printing. Patterns are printed one slice at a time. (c) The optical setup: FR = Faraday rotor, EOM = Electro-optic modulator, SM = x-y Galvanometer scanning mirrors, SL = Scan lenses and beam expander, DM = Dichroic mirror, PZ = piezo z-mount. Image obtained from Scott¹.

1.2.3 Schematic for printing biotinylated proteins in scaffold materials

To print the patterns of biotinylated proteins inside scaffolds, the scaffolds materials can be prepared by sandwiching the prepolymer solution between adhesion promoting and adhesion

resistant glass slides (Fig 1.4a). After gelation of scaffolds, the adhesion resistant coverslip is removed and B4F solution is added to diffuse into the scaffolds, and the gelled scaffolds are ready for printing (Fig 1.4b). After mounting the glass slides with scaffolds on the stage of femtosecond laser 3-D microprinting system, the laser is scanned in x, y, z to photocrosslink B4F. Upon excitation, B4F binds to the adjacent scaffold materials (Fig 1.4c). After printing, the unbound B4F is rinsed out with PBS, and streptavidin is added to bind to the patterned biotin moieties (Fig 1.4d). After rinsing with PBS to remove the unbound streptavidin, the biotinylated proteins can be added to bind to the remaining biotin binding sites on the streptavidin (Fig 1.4e). Finally, after rinsing out the excess biotinylated protein, the patterns of biotinylated proteins are generated (Fig 1.4f).

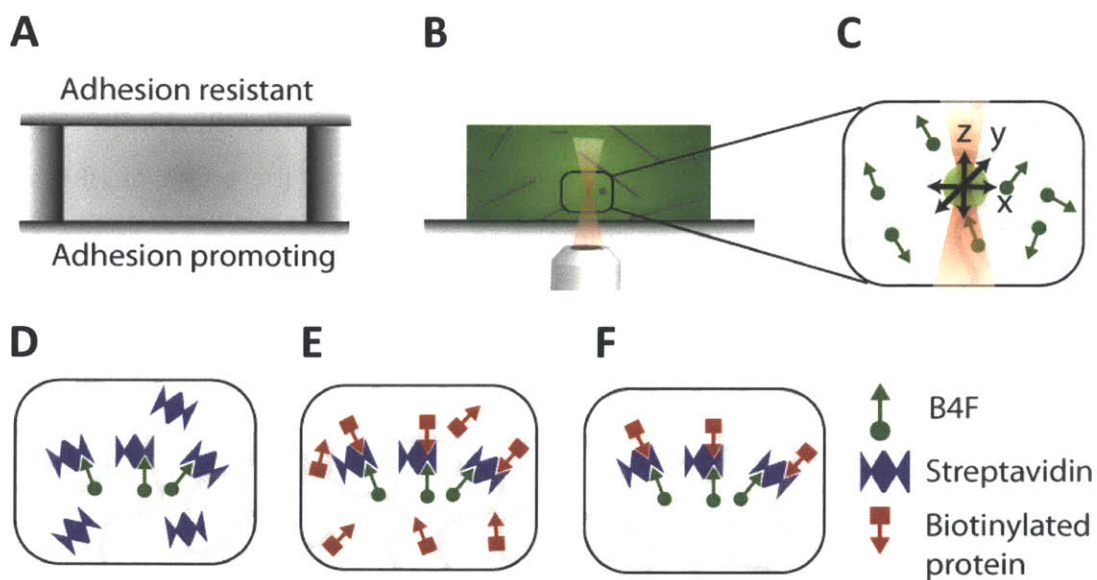


Fig 1.4: Printing proteins in three-dimensional scaffolds. (a) The collagen prepolymer solution is gelled between adhesion resistant glass and adhesion promoting glass. (b) The gelled collagen is diffused with B4F, and (c) laser is scanned in x, y, z to photocrosslink B4F. After printing, (d) streptavidin and (e) biotinylated proteins are added sequentially. (f) After washing out excess biotinylated proteins, the patterns of proteins are generated. Image obtained from Scott¹.

1.2.4 Patterns of streptavidin formed in scaffold materials

Using the printing process described above, several materials of scaffolds have been demonstrated to be 3-D patterned with streptavidin, such as collagen, gelatin methacrylate, fibrin and agarose scaffolds. The pattern brightness varies between scaffold materials. In addition, the pattern brightness can be increased via acrylation modification of scaffold materials. The patterns can also be formed in variable porosity collagen scaffolds. The pattern brightness varies with laser power, and has an axial resolution of $\sim 5\mu\text{m}$ in collagen scaffold and $\sim 10\mu\text{m}$ in gelatin methacrylate, fibrin and agarose scaffolds. The gradient formation of biotinylated proteins can be achieved by continuously varying laser power using EOM (Fig 1.5a). Fig 1.5b shows the arbitrary 3-D patterns of streptavidin in fibrin scaffolds. A pyramid, a cube, and a sphere with a diameter of $110\mu\text{m}$ were printed with streptavidin patterns formed in approximately 8 seconds. To show the biotinylated protein can both bind to the patterned streptavidin and retain its biological activity after binding, the biotinylated horseradish peroxidase (HRP), an enzymatically active protein, was added to bind to the streptavidin patterns (Fig 1.5c). Upon the addition of amplex red, the enzymatic action of HRP showed a pattern of amplex red fluorescence, which matched the patterns of streptavidin fluorescence (Fig 1.5d).

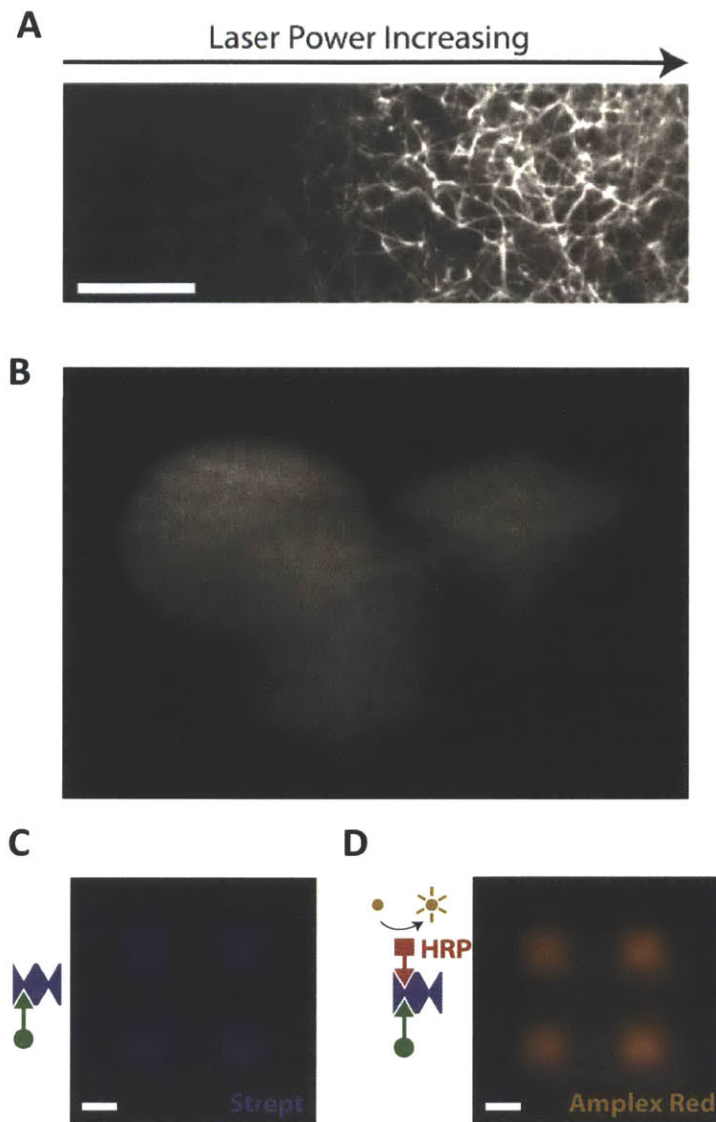


Fig 1.5: Patterns of streptavidin formed in scaffold materials. (a) Smooth gradients prepared in a collagen scaffold by variation of laser power across scanlines. Scale bar = 20 μ m. (b) 3-D printed shapes in a fibrin scaffold. Print time is 8 seconds per shape. (c)(d) Patterns of streptavidin and amplex red fluorescence to demonstrate printing of enzymatically active biotinylated protein. Scale bar = 50 μ m. Image obtained from Scott¹.

1.2.5 3-D Printing of Collagen Scaffolds by Photobleaching of Fluorescein

The 3-D printing of collagen scaffolds has been demonstrated by photobleaching of the fluorescein infused collagen gel. As mentioned before, fluorescein is able to crosslink the

scaffold materials by binding to the nearby surface upon excitation. The pregelled, fibrillar collagen scaffolds were hypothesized to have higher probability of crosslinking, leading to higher printing speeds. As a result, using the femtosecond laser system in Fig 1.3c, the multiphoton photobleaching of fluorescein can be performed to crosslink the collagen.

The pregelled collagen can be prepared as described in 1.2.3, and then fluorescein is added to diffuse into the collagen. After printing the 3-D microstructure in the fluorescein infused collagen (Fig 1.6a,i), the collagen is rinsed out the excess fluorescein with PBS. A developer solution is then added to solubilize the uncrosslinked collagen. The developer solution can be 0.2M acetic acid with pH 3.5 or 1M tris-HCl buffer with pH7.4. The development of collagen scaffold in acetic acid is stronger than tris-HCl buffer. After development, the 3-D microstructure of collagen scaffolds can be revealed (Fig 1.6a,ii). The A printed elephant of collagen scaffolds is shown in Fig 1.6b, which demonstrated the high-resolution printing of this method. One feature of this printing technology is the shrinkage of the collagen scaffold upon developing. The degree of shrinkage varying with the collagen gel density and the incident laser power used to crosslink the collagen.

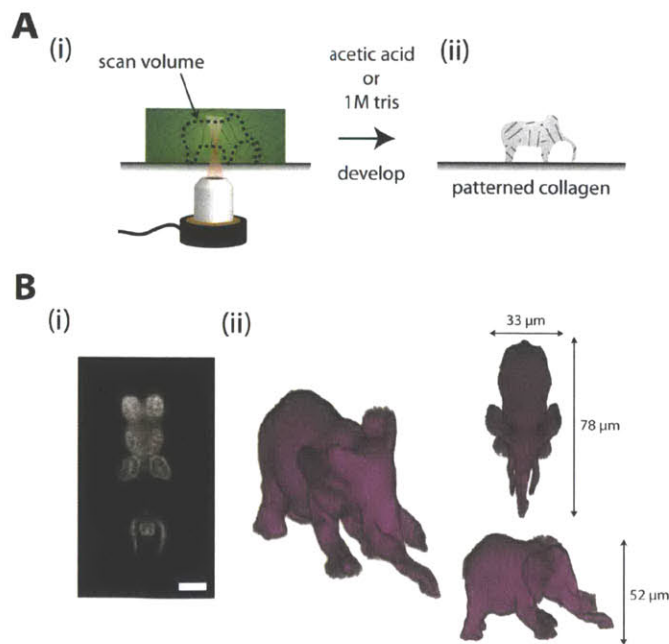


Fig 1.6: 3-D printing of collagen scaffolds. (a) A fluorescein infused collagen gel is printed by the femtosecond laser, and acetic acid or

tris-HCl is added to dissolve unexposed regions. (b) Arbitrary shape of an collagen elephant is printed. The printing time is about 5 sec. Image obtained from Scott¹.

1.2.6 Combined Printing of Scaffolds and Internal Protein Cues

3-D printing of proteins in scaffolds and 3-D printing of scaffolds can be combined together to create a rapid 3-D laser microprinting technique that can print both the microarchitecture of scaffolds and internal protein patterns. This technique can be performed by first printing a volume of fluorescein infused pregelled scaffold material, and then diffusing B4F solution into the printed gel and printing a second volume with biotin moieties. After removing the printed scaffold from the stage and rinsing out the excess B4F, acetic acid is added to develop the microstructure of scaffold. After development and neutralization by PBS, streptavidin is added to bind to the biotin moieties on B4F patterns (Fig 1.7a). The biotinylated proteins can be added to bind to the remaining biotin binding site to generate the internal protein patterns. Using this technique, the scaffolds with independent microarchitectures and internal protein patterns can be created (Fig 1.7b). One advantage of this technique is that no 3-D alignment is necessary to align the internal patterns of protein to the patterned scaffolds since we can carefully add B4F that the sample is not moved.

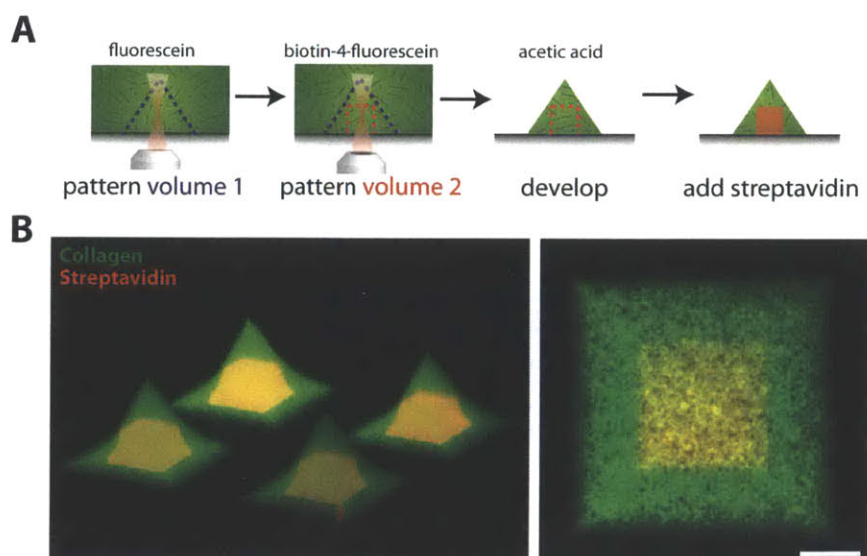


Fig 1.7: Printing proteins inside 3-D printed collagen scaffolds. (a)

Method for printing scaffold microarchitecture and internal patterns of proteins. (b) Printed collagen shapes containing internal patterns of streptavidin. Scale bar = 20 μ m. Image obtained from Scott¹.

1.3 Scope of thesis work

We've discussed the rapid 3-D laser microprinting technique developed by Scott. The femtosecond laser system is able to perform printing defined 3-D microarchitecture of scaffold materials and simultaneously printing 3-D patterns of protein cues inside the scaffold. Such ability is promising in several applications, such as creating engineered tissue with high complexity for regenerative medicine and building a biomimetic microenvironment for biology research or drug screening assays. Although the rapid 3-D laser microprinting technique has been presented to have effective printing results, the biological activity involved in printed scaffolds and printed proteins has not yet been studied, and the biological activity or functions of printed scaffolds and printed proteins are crucial for the development of future applications.

The objective of this thesis is to further develop the technique of rapid 3-D laser microprinting by researching on the biological activity and functions of printed scaffolds and printed proteins. Several biological assays were conducted inside the printed scaffolds with printed proteins, while these assays revealed some potential applications of the technique.

The second chapter introduces an in-vitro leukocyte rolling system developed by the rapid 3-D laser microprinting technique. The system is a microfluidic device containing printed collagen scaffolds with printed internal P-selectin patterns. HL-60 leukocytes rolling on P-selectin patterned collagen channel demonstrated that printed protein cues retain their biological activity.

The third chapter introduces a 3-D printed microvasculature, which was developed by seeding endothelial cells into the defined microarchitecture within collagen scaffolds. The leukocyte rolling assay described in the second chapter was implemented again in the 3-D printed microvasculature to further prove the properties and functions of the rapid 3-D laser microprinting.

The fourth chapter introduces guiding and homing of cells inside a 3-D microprinted collagen scaffolds. Guiding and homing of cells is the first step to create an engineered stem cell niche in the future. During the development of design, the rapidly prototyping process could be easily achieved by the rapid 3-D laser microprinting technique.

The last chapter summarizes and concludes the thesis work and suggests the potential future work for the rapid 3-D laser microprinting technique.

Chapter 2: 3-D MICROPRINTED COLLAGEN SCAFFOLDS CONTAINING INTERNAL P-SELECTIN PATTERNS FOR LEUKOCYTE ROLLING ASSAY

In this chapter, we introduce an in-vitro leukocyte rolling system developed by the rapid 3-D laser microprinting technique. The in-vitro leukocyte rolling system is a microfluidic device containing printed collagen scaffolds with printed internal P-selectin patterns. We demonstrate HL-60 leukocytes rolling on printed P-selectin, which proves that the printed protein cues of rapid 3-D laser microprinting method retain their biological activity.

2.1 Background and Motivation

2.1.1 Leukocyte recruitment occurring to the vascular wall

Leukocyte recruitment from blood circulatory system towards sites of inflammation is an essential immune response in human body¹⁸. Leukocyte recruitment is the early event of acute and chronic inflammation; immune surveillance of tissue; and wound defense and repair, so leukocyte-endothelial interaction in the process of leukocyte recruitment has been studied extensively¹⁹. Fig 2.1 shows the well-accepted multistep process of leukocyte recruitment occurring to the vascular wall²⁰. First, circulating leukocytes in the bloodstream tether and roll on activated endothelium via selectin-mediated or some integrin-mediated mechanisms²¹. Second, integrins on leukocyte surface are activated by chemokines or other proinflammatory sources released by various sources within the tissue (such as mast cells or tissue macrophages), and the integrin activation leads to firm adhesion²². Finally, firm adhesion permits leukocyte transmigration cross the endothelium, which involves interaction with endothelial junctional proteins, and then leukocytes are able to move towards the inflamed tissue²³.

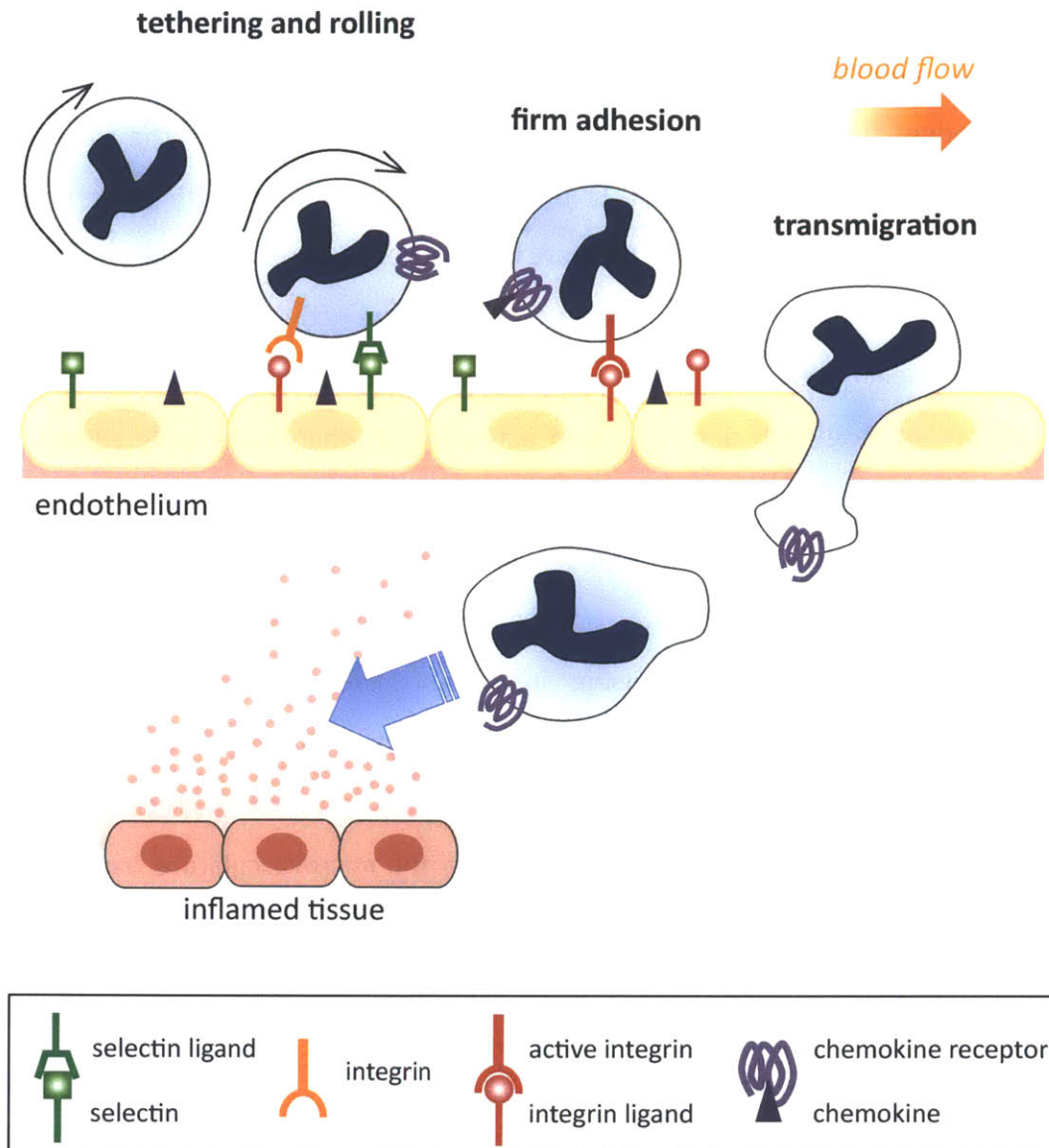


Fig 2.1: A multistep process of leukocyte recruitment. Circulating leukocytes first tether and roll on activated endothelium by selectin-mediated or some integrin-mediated mechanisms. Chemokine activates integrin on leukocyte, leading to firm adhesion. Finally, firm adhesion permits leukocyte transmigration cross the endothelium, and leukocyte is able to move toward the inflamed tissue. Image adapted from Kunkel et al²⁰.

2.1.2 Selectins are the main roles in leukocyte rolling

Rolling is the first step of leukocyte recruitment. It initiates the fast-moving leukocytes in the

bloodstream to slow down, and $\beta 2$ integrins on slow-down leukocytes have chance to be activated by nearby chemokines or other proinflammatory sources²⁴. Selectins, calcium-dependent transmembrane glycoproteins, are the main roles in the rolling process²⁵. P-selectin glycoprotein ligand-1 (PSGL-1) is the ligand interacting with selectins, and it is expressed on almost all leukocytes²⁶. There are three types of selectins: L-selectin, expressed by leukocytes, mediates leukocyte-leukocyte interactions; E-selectin and P-selectin, expressed by activated endothelial cells, mediates leukocyte-endothelial interactions²⁷. The detailed mechanisms about P-selectin and E-selectin activation of endothelial cells will be discussed further in *Chapter 3*. There are many studies researching on the detailed mechanisms of leukocyte rolling²⁸⁻³⁰. In-vivo and in-vitro leukocyte rolling experiments have been designed and conducted. In-vivo studies of leukocyte rolling along the vascular endothelium of postcapillary venules has been researched by using intravital microscopy, and in-vitro studies of selectin-mediated leukocyte rolling has been researched by conducting flow chamber assay^{31,32}. In addition to the different types of ligands involved in leukocyte rolling process, the fluid shear stress of blood flow and the selectin site densities in the microvasculature have been studied for the biomechanics of leukocyte rolling³³⁻³⁵.

2.1.3 Use the rapid 3-D laser microprinting technique to create an in-vitro leukocyte rolling system

The rapid 3-D laser microprinting technique is able to create 3-D printed scaffolds containing internal 3-D patterns of proteins. In order to prove the printed protein cues retain their biological activity, printed horseradish peroxidase has been demonstrated to preserve the enzymatic action upon the addition of amplex red (see *Chapter 1*). Here, we want to further prove the biological activity of printed protein cues interacting with cells. Since leukocyte rolling has been studied extensively and the binding of PSGL-1 and selectins has been well investigated, we chose to establish a leukocyte rolling system using our rapid 3-D laser microprinting technique. A capillary-like 3-D microstructure could be created by printing of scaffolds, while the selectin ligands could be patterned onto desired position inside the printed scaffolds. The

cell rolling occurring on the 3-D printed protein patterns inside scaffolds could determine the biological interaction between the printed selectin ligands and PSGL-1 on leukocytes. Therefore, presenting the leukocyte rolling in our system could demonstrate that the biological properties and functions of 3-D printed proteins are preserved.

2.2 Results

2.2.1 Schematic for leukocyte rolling system

PSGL-1 and P-selectin binding is a well-understood mechanism in leukocyte rolling, so we simplified the leukocyte rolling process to be as Fig 2.2a: PSGL-1 on leukocytes binds to P-selectin ligands on endothelial cells, and the binding enables the rolling. By using the rapid 3-D laser microprinting technique described in *Chapter 1*, a simple leukocyte rolling system was presented here (Fig 2.2b). After printing desired collagen scaffold microstructures, B4F was photocrosslinked onto locations of collagen scaffold where rolling took place. Streptavidin was added to bind to the patterned biotin moieties. Finally, biotinylated P-selectin was added to bind to the streptavidin-biotin sites. Leukocyte rolling occurred on patterned P-selectin ligands by flowing leukocytes through collagen scaffolds. The performance of leukocyte rolling depends on the density of P-selectin sites, which can be controlled by laser power for B4F patterning.

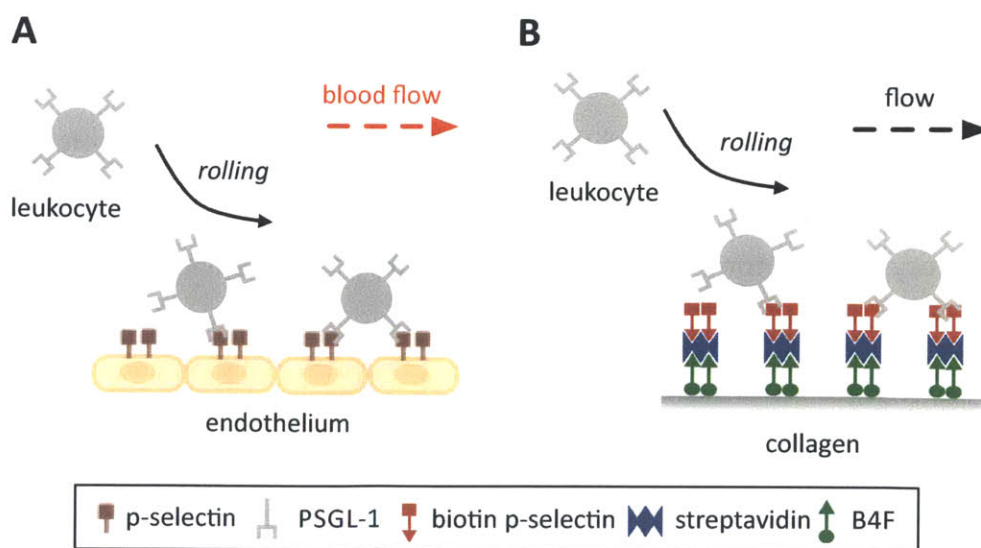


Fig 2.2: Leukocyte rolling process. (a) A simplified leukocyte rolling process that leukocytes roll on the endothelium because of the binding of PSGL-1 and P-selectin. (b) Using the 3-D laser microprinting method, B4F was first photocrosslinked by laser and streptavidin was added to bind to B4F followed by the addition of biotinylated P-selectin. The binding of biotinylated P-selectin and streptavidin generated the P-selectin patterns providing leukocyte rolling.

For flowing cells into the leukocyte rolling system, a PDMS microfluidic chip was designed as Fig 2.3a. Two wells with a diameter of 6 mm were connected with a $1\text{mm} \times 500\mu\text{m} \times 150\mu\text{m}$ (length \times width \times height) channel. Collagen was injected into the channel and gelled at 37°C . The PDMS microfluidic chip was put on the stage of fast 3-D laser microprinting system, and printing was performed in the gelled collagen. All chemical solutions involved in the whole 3-D laser microprinting process (i.e. fluorescein, B4F, acetic acid, PBS, BSA, streptavidin, biotinylated P-selectin, and media for leukocytes) could be diffused into the collagen scaffolds by filling into two wells, and also be flowed into the collagen scaffolds by simply adding a small amount of liquids in one well to create a pressure drop. While performing leukocyte-rolling experiments, the flow of leukocytes could be driven by this method.

The collagen scaffold microstructure consisted of two identical branched channels with a diameter of $50\mu\text{m}$ as shown in Fig 3b. The size of whole microstructure was $700 \times 500 \times 150\mu\text{m}$ (length \times width \times height) printed in 5 rows and 7 columns of $100 \times 100 \times 150\mu\text{m}$ sections. One of branched channels was printed with an annular pattern of P-selectin. The size of the annular pattern was designed with an inner diameter of $46\mu\text{m}$ and an outer diameter of $66\mu\text{m}$ to ensure P-selectin ligands were printed on the surface of channels. The patterned branched channel is leukocyte rolling zone, and the unpatterned branched channel is the control zone.

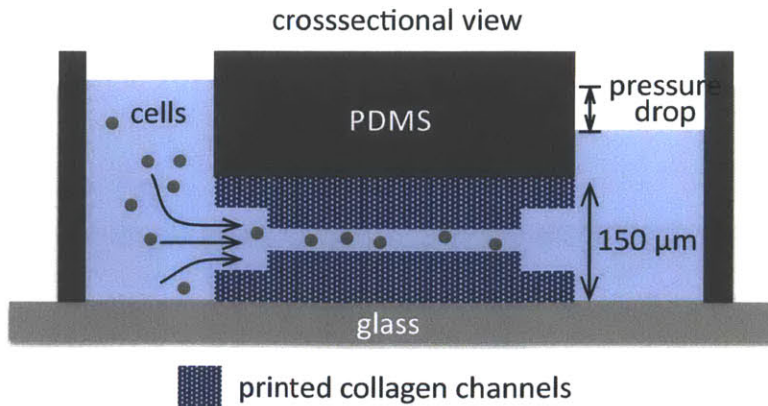
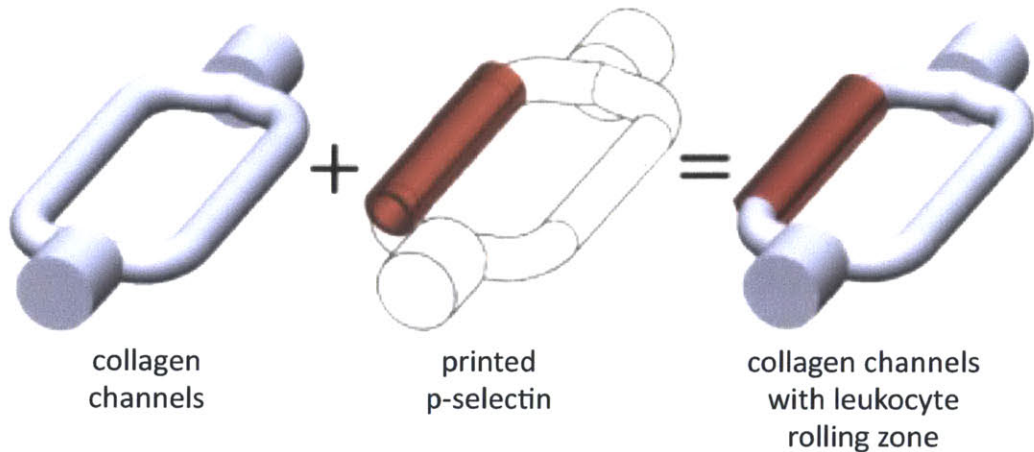
A**B**

Fig 2.3: The device of leukocyte rolling system. (a) A PDMS microfluidic chip was injected with collagen prepolymer into the channel and gelled at 37°C. After gelation, the chip was put on the stage of the rapid 3-D laser microprinting system for printing inside the collagen gel. Applying additional amount of liquid in one well could provide a pressure drop for flowing the cells into the channel. (b) The geometries of collagen channels and P-selectin patterns provide a leukocyte rolling zone and a control zone.

2.2.2 Performance of 3-Dleukocyte rolling system

The printed collagen scaffolds were imaged as shown in Fig 2.4. The fluorescent green was collagen, and the fluorescent orange was streptavidin. The microstructure can be seen clearly in Fig 2.4a. The leukocyte rolling zone was well distinguished from the control zone by the high contrast of streptavidin patterns. The grid-like patterns in Fig 2.4a were due to sectional

printing. The cross-sectional view in Fig 2.4b shows that the streptavidin patterns were well bound to the surface of collagen channels. Fig 2.4c shows the enlarged view of collagen channels.

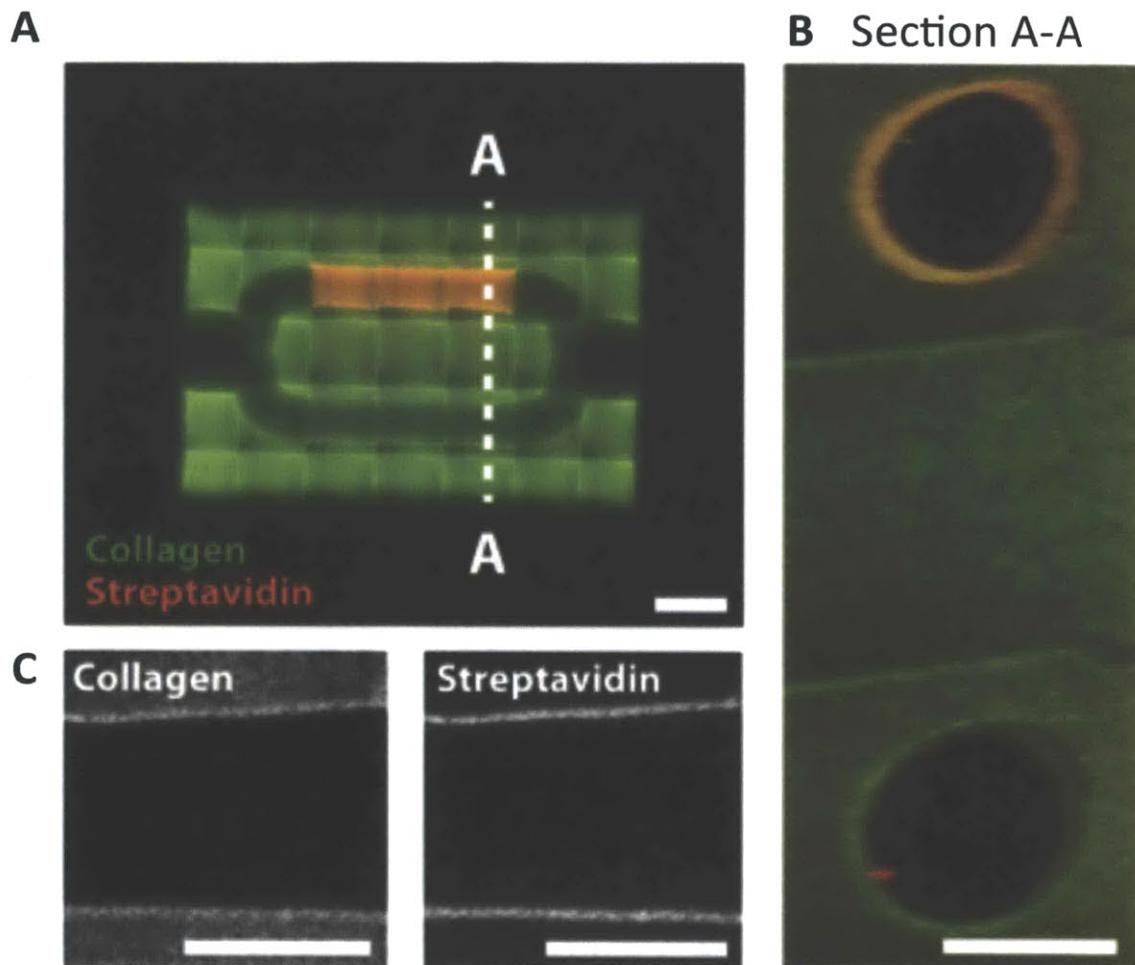


Fig 2.4: Collagen channels containing a region printed with streptavidin. (a) Scale bar = 100 μ m. (b) Cross-section of channels acquired from two-photon imaging, scale bar = 50 μ m. (c) Two-photon images of printed collagen and streptavidin, scale bar = 50 μ m.

In order to test the performance of this leukocyte rolling system, HL-60 leukocytes were flowed into the collagen channels. Videos were recorded during the HL-60 leukocyte rolling experiments. Upon addition of HL-60 leukocytes, cell rolling occurred on the P-selectin printed branch, but not on the unpatterned branch. In Fig 2.5, the white arrow points a HL-60 leukocyte

rolling on P-selectin. After 4 seconds, the rolling cell traveled about 80 μ m. The black arrow points another HL-60 leukocyte flow through the unpatterned channel without rolling. The non-rolling cell passed through the whole branch (~500 μ m) in 4 seconds. The significant difference in speed indicated the printed P-selectin functioned as normal. The P-selectin ligands on collagen scaffolds were able to bind to PSGL-1 receptors on HL-60 leukocytes.

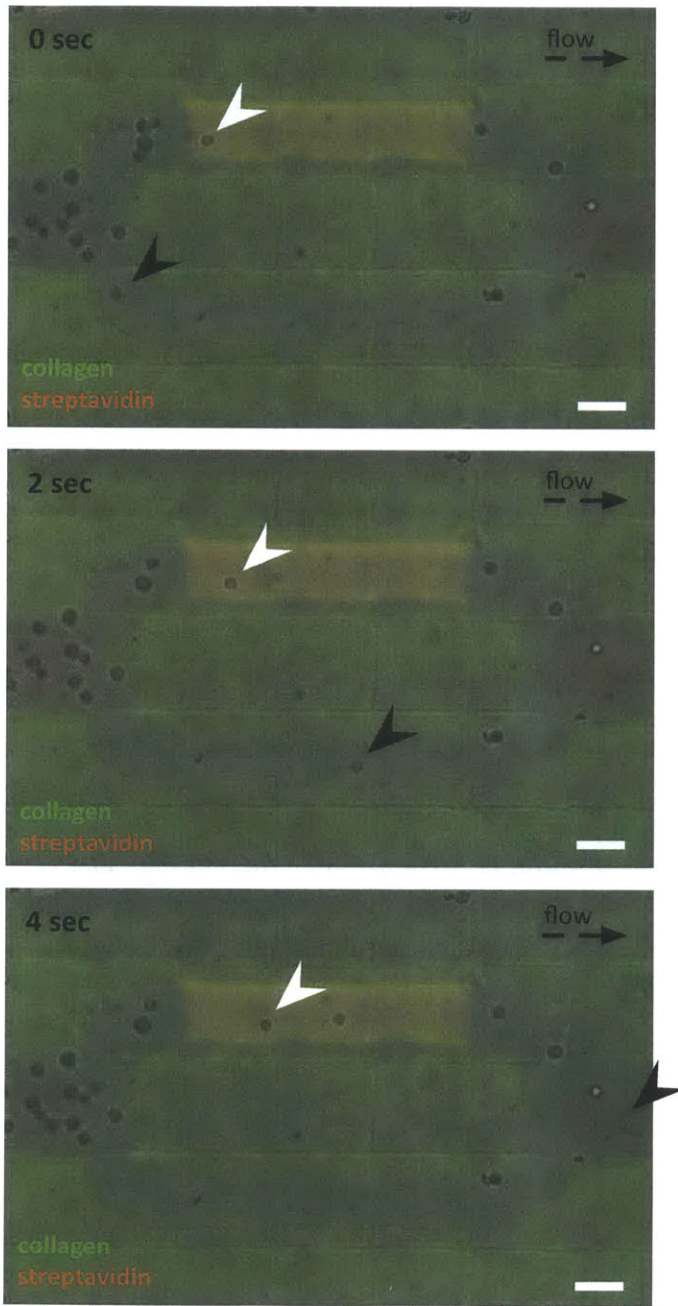


Fig 2.5: HL-60 leukocytes rolling on patterned collagen channel. In 4 seconds, a HL-60 cell (the white arrow) rolled on P-selectin patterned collagen channel traveling about 80 μ m, while the other HL-60 cell (the black arrow) flowed through unpatterned channel traveling about 500 μ m. Scale bar = 50 μ m.

2.2.3 HL-60 leukocyte rolling assay

To further prove HL-60 leukocyte rolling was caused by the printed P-selectin binding to PSGL-1 receptors on HL-60, two different control groups were performed. One control group was blocking PSGL-1 receptors on HL-60 leukocytes by pre-incubating HL-60 cells with soluble P-selectin (Fig 2.6b). Another control group was patterning the channels only with streptavidin (i.e. without biotinylated P-selectin) for HL-60 leukocyte rolling (Fig 2.6c). One experimental group (Fig 2.6a) and two control groups (Fig 2.6b, c) were repeated for 3 to 4 times. The control groups of blocking PSGL-1 receptors were performed right after experimental groups (i.e. in the same chips). HL-60 cell rolling ratio was determined by the ratio of the number of rolling cells in a branch to the total number of cells that flowed through the branch.

Fig 2.6 shows the results of three groups. The HL-60 cell rolling ratio of the experimental group (Fig 2.6a) was 29% \pm 11% on patterned branch and 2% \pm 3% on unpatterned branch. The cell rolling ratios of two control groups (Fig 2.6b, c) were all 0%, except the ratio on unpatterned branch of Fig 6c control group, which was 1% \pm 1%. There were significant differences between the rolling ratio on patterned branch of experimental group and the rolling ratio on the all other branches in experimental group and control groups. The average cell rolling speed was about 5.8 μ m/sec.

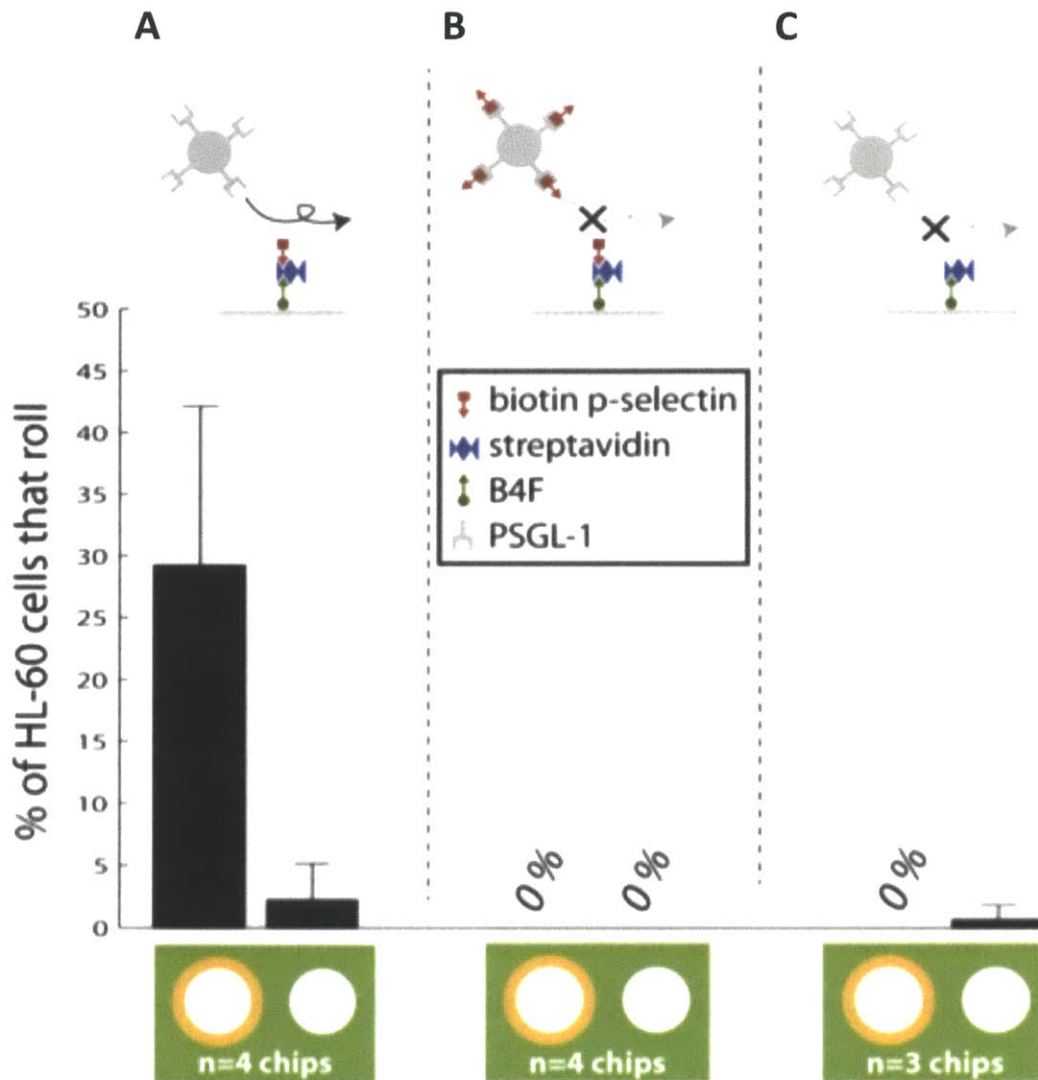


Fig 2.6: Percentage of HL-60 rolling ratio, which is the ratio of rolling cells to the total number cells flowed through a branch on (a) P-selectin patterned and unpatterned collagen channels; (b) the same channels, but the HL-60 cells are pre-incubated with soluble P-selectin; (c) printed collagen channels coated with streptavidin only.

2.3 Discussion

In this 3-D leukocyte rolling system, the HL-60 cell rolling can be observed on the P-selectin patterned branch. The cell rolling speed was about 35 times smaller than the cell flow rate. This big difference in speed indicated a prominent presence of cell rolling. From the quantitative

results of experimental group, the significant difference in HL-60 cell rolling ratio between P-selectin patterned and unpatterned branch showed that rolling occurred due to the pattern of P-selectin. By eye observation, once HL-60 cells touched the surface of P-selectin patterns, they had high chance to roll. Therefore, the cell rolling ratio of 29% could be thought to be the percentage of cells touching the surface (i.e. the remaining percentage of cells were just flow through the middle of the branched channel). The quantitative results of two control groups could be concluded that the blocking of PSGL-1 receptors on HL-60 cells inhibited rolling, and channels patterned only with streptavidin did not elicit HL-60 cell rolling. This means the rolling involved P-selectin binding to PSGL-1 on HL-60 cells, and the rolling was not caused by the affinity of streptavidin.

In the quantitative results, there was a cell rolling ratio of 1-2% in the unpatterned branch of the experimental group and one control group. This small rolling ratio might be caused by several possible reasons. First, when streptavidin or biotinylated P-selectin were added into the channels after printing, there was non-specific binding everywhere in collagen scaffolds. This non-specific binding could be observed from the background intensity of fluorescent streptavidin, which was pretty low. In spite of this, the sum of non-specific binding sites of streptavidin and biotinylated P-selectin still give HL-60 cells the chance for rolling. To solve the problem of non-specific binding, we can either increase the washing time after the addition of streptavidin and biotinylated P-selectin, or increase efficiency of blocking procedure before the addition of streptavidin (see *Detailed Methods*). The second possible reason for the small rolling ratio was the chance that HL-60 cells stick to collagen or trapped by some defect of collagen surface. This problem is hard to avoid. However, we've set that cells were counted as rolling if they remained adhered to the wall for more than 100 μ m (see *Detailed Methods*). Thus, the small cell rolling ratio might be cancelled if we increase the criteria of 100 μ m.

With the rapid 3-D laser microprinting technique, collagen scaffolds with defined microarchitectures and internal micropatterns of proteins can be printed together. An in-vitro leukocyte rolling system can be easily created by this method. The capillary shape

microstructures allow a more precise simulation of in-vitro environment for leukocyte rolling. The specific leukocyte rolling zone can be assigned easily by this technique, so an experimental group and a control group can be implemented simultaneously in one chip. Most of all, the performance of leukocyte rolling experiments proved that the printed proteins (i.e. P-selectin) functioned normally. The printing method still retains the original biological activity and characteristics of the printed proteins, and it suggests a potential application for drug screening assays in biomimetic environment.

2.4 Conclusion

We have demonstrated an in-vitro leukocyte rolling system by using the rapid 3-D laser microprinting technique. The results showed HL-60 leukocyte rolling occurred on printed P-selectin patterns. The leukocyte rolling system proved that the printed proteins from the rapid 3-D laser microprinting technique retain the original biological activity and functions.

2.5 Detailed Methods

2.5.1 Fabrication of PDMS microfluidic chips

The PDMS microfluidic chips were fabricated using well-developed soft lithography replica molding techniques. SU-8 2050 (MicroChem, Newton, MA) was spun at 1250 rpm for 30 seconds to generate a 150 μ m film on a wafer, softbaked at 65 $^{\circ}$ C for 5 min and 95 $^{\circ}$ C for 25 min, exposed to UV through a printed transparency, postbaked at 65 $^{\circ}$ C for 5 min followed by 95 $^{\circ}$ C for 10 min. The patterns were developed in PM acetate, and hard baked at 150 $^{\circ}$ C for 15 min. The wafer was then silanized by (Tridecafluoro-1,1,2,2-tetrahydrooctyl)-1-trichlorosilane in a desiccator for 10 min. Sylgard 184 was mixed with its crosslinker at a 10:1 ratio, cast onto the SU-8 patterned wafer, degassed for 1hr in a desiccator, and cured at 70 $^{\circ}$ C for 1hr. After removing the cured PDMS from wafer, two 6 mm diameter wells were punched by a biopsy punch. The PDMS chip was plasma bonded to a 100 μ m thick glass coverslip.

2.5.2 Collagen scaffold preparation

A collagen prepolymer solution containing collagen at 7.5 mg/ml was prepared by neutralization of a high concentration stock solution of rat tail collagen I (BD Biosciences, San Jose, California) with PBS containing 125mM of HEPES (pH 7.4). The collagen prepolymer solution was then pipetted directly into the channel of the PDMS microfluidic chip right after the plasma bonding of chip and glass coverslip, and gelled in an incubator at 37°C for 30 min.

2.5.3 Printing collagen scaffolds

The microstructure of collagen scaffolds was designed in SolidWorks (Dassault Systèmes SolidWorks Corporation, Waltham, MA). The design was uploaded to our 3-D laser microprinting system (see *Chapter 1*).

Before printing, 200 µg/ml of fluorescein (JT Baker) in PBS was added into two wells of the microfluidic chip for diffusion, and removed after 1hr. The chip was then put on the stage of the 3-D laser microprinting system. A collagen structure (700 × 500 × 150µm) was printed in 5 rows and 7 columns of 100 × 100 × 150µm sections that comprise the complete structure. Each section was printed in about 8 sec, finishing the whole structure in about 5 min. After printing the microstructure, the wells were filled with 200 µg/ml of B4F (Life Technologies, Carlsbad, CA) in PBS for diffusion for 1hr. Here, care was taken not to displace the chip on the stage, such that no 3-D alignment was necessary for next-step printing of protein patterns. The annular structure for P-selectin patterns was then printed, which only took about 25 sec. After B4F patterning, B4F was rinsed out with PBS, which was then replaced by acetic acid to develop the collagen channels. After 1hr of development, acetic acid was rinsed out and neutralized with PBS, and replaced by 3% wt/wt BSA (Fisher Scientific) in PBS for blocking. After 1hr of blocking, 10 µg/ml of streptavidin in 3% BSA was added into the wells. After 1hr of streptavidin binding, the unbound streptavidin was rinsed out with PBS for 30 min. Next, the prepared biotinylated P-selectin (P-selectin, R&D system) was added at 10 µg/ml in 3% BSA. After 1hr of P-selectin binding, the unbound P-selectin was rinsed out with PBS for 30 min. The chip was then ready

for leukocyte rolling experiments.

2.5.4 Cell culture

HL-60 cells were cultured in flasks in an incubator at 37°C with 5% CO₂, using IMDM (Life Technologies) with 10% FBS containing 100U/ml penicillin/streptomycin (Life Technologies).

2.5.5 Leukocyte rolling assay

When the microfluidic chip was ready for leukocyte rolling experiments, the collagen channels were first equilibrated with the HL-60 cell culture media, and 2µl of HL-60 cells were added to one well to drive a flow of cells through the channels. For consistency of flowing profile, this process was used in every rolling experiment. The 2µl of HL-60 cell flowing would take 4 to 5 minutes to reach equilibrium. Only 120 seconds with average cell flow rate of 200µm/sec were taken into account. Cells were counted as rolling if they remained adhered to the wall for > 100µm along the straight section of P-selectin patterned or unpatterned branch. From this count, a cell rolling ratio was calculated as the ratio of the number of rolling cells in a branch to the total number of cells that flowed through the branch.

For the control group of blocking PSGL-1 receptors on HL-60 leukocytes, HL-60 cells were pre-incubated with 10µg/ml of P-selectin in HL-60 culture media for 30 minutes. The other control group was prepared the same as the experimental group.

2.5.6 Image and data analysis

Three-dimensional images of collagen channels with leukocyte rolling zone were obtained using a two-photon fluorescence microscope (Prairie Technologies, Middleton, WI) using a MAI-TAI laser. Collagen scaffolds for two-photon imaging were fluorescently conjugated by 50 µg/ml DyLight 488 (Thermo Scientific) in borate buffer (pH 8) for 5 minutes, and then rinsed out with PBS to remove unconjugated dye. Streptavidin for two-photon imaging was an Alexa-Fluor 594 conjugated streptavidin (Life Technologies).

Videos were taken under microscope during HL-60 leukocyte rolling experiments. The cell numbers and cell rolling numbers were counted by eye observation. The cell flow rate and cell rolling speed were determined by the ratio of cell traveling length to cell traveling time.

Chapter 3: 3-D PRINTED MICROVASCULATURE AND LEUKOCYTE ROLLING ASSAY

In this chapter, we demonstrate a 3-D printed microvasculature developed by the rapid 3-D laser microprinting technique. The 3-D printed microvasculature was formed by seeding human umbilical-vein endothelial cells (HUVECs) into a 3-D printed collagen scaffolds. We also show a leukocyte rolling assay performed in the 3-D printed microvasculature. The leukocyte rolling assay helped to further prove the properties and functions of the rapid 3-D laser microprinting.

3.1 Background and Motivation

3.1.1 The role of vascularization in tissue engineering

The construction of engineered tissue provides solutions to restore, maintain or improve tissue function or a whole organ⁴. Some of engineered tissues have already been used for clinical use, such as engineered skin and cartilage, while researchers have studied many other potential tissue types, such as liver, bone, muscle, adipose and nervous tissues³⁶. When incorporating the engineered tissue back into the host, depending only on diffusion provides very limited incorporation³⁷, except skin and cartilage tissue, which have relatively low demands for nutrients and oxygen and diffusion is sufficient for them³⁶. Vascular network plays an important role in carrying oxygen and nutrients to tissue. Therefore, when it comes to more complex and larger tissues compared to skin and cartilage, one of important and challenging problems is vascularization in those complex engineered tissue^{38,39}.

Rouwkema et al. presented a review of vascularization in tissue engineering, in which they categorized the method of vascularization into: scaffolds design, angiogenic factor delivery, in-vivo prevascularization and in-vitro prevascularization⁴⁰. In the paper, they determined the speed of vascularization of a tissue-engineered construct after implantation at a defect site could further prioritize the four categories, from in-vivo prevascularization, in-vitro prevascularization, angiogenic factor delivery to scaffold design. In-vivo prevascularization is the most promising method that the construct can be perfused immediately after implantation.

However, the additional surgery is needed for the preparation of in-vivo prevascularization in the construct^{41,42}. In-vitro prevascularization has been demonstrated to accelerate the connection between the prevascular networks and the host vascular system after implantation^{43,44}. Although these two methods of prevascularization are more promising, the scaffold design and angiogenic factor delivery involved in the design of construct are still critical for allowing host vasculatures to grow into the construct⁴⁰.

Here, utilizing the advantage of our rapid 3-D laser microprinting technique, in-vitro prevascularization can be achieved by creating the defined microarchitecture inside scaffold materials. The capillary-like microstructures can be first printed, and the microvasculature inside scaffolds can be created by seeding endothelial cells into the microstructures. Furthermore, combining printing of scaffolds with printing of internal protein patterns inside scaffolds may provide a promising tool for scaffold design and angiogenic factor delivery, which are important for vascularization as mentioned above.

3.1.2 Leukocyte rolling assay within printed microvasculature

The leukocyte rolling assay described in *Chapter 2* provided the idea to implement the leukocyte rolling assay within printed microvasculature. After creating the microvasculature inside scaffolds using the rapid 3-D laser microprinting method, we implemented the leukocyte rolling assay in the printed microvasculature to demonstrate further in leukocyte-endothelial interaction in leukocyte recruitment.

In *Chapter 2*, we've discussed about the process and the importance of leukocyte recruitment and the mechanisms of leukocyte rolling. Selectins are the main roles in leukocyte rolling. The activated endothelium expresses P-selectin or E-selectin ligands for leukocyte rolling, and P-selectin glycoprotein ligand-1 (PSGL-1) is the ligand on leukocytes binding to P-selectin and E-selectin. P-selectin and E-selectin expression on endothelial cells can be induced by many different agents. The inducing agents for P-selectin include thrombin, histamine, complement fragments, oxygen-derived free radicals, cytokines, lipopolysaccharide (LPS), and TNF- α , while

the inducing agents for E-selectin include IL-1, TNF- α , interferon- γ , substance P and LPS⁴⁵. All these inducing agents are important for activation of endothelium in the inflammatory response. Therefore, applying these inducing agents to the printed microvasculature leads to the activation of endothelial cells and enables the leukocyte rolling.

The leukocyte rolling on activated endothelium assay could be conducted by printing the inducing agents inside the printed scaffolds with defined microarchitecture, the microvasculature could be created, while printed inducing agents were able to activate the endothelial cells within the microvasculature. This rolling assay within printed microvasculature could further demonstrate that the printed proteins using the rapid 3-D laser microprinting technique retains their biological activity and functions. Furthermore, it could also prove that the printed microvasculature preserves the biological functions.

3.2 Results

3.2.1 3-D printed microvasculature

To create microvasculature using rapid 3-D laser microprinting technique, we used the same design of the PDMS microfluidic device in *Chapter 2* (Fig 2.3a), which contained the collagen scaffolds for printing and allowed to drive a flow within the collagen scaffolds for endothelial cell seeding. We also chose the same geometry of 3-D microarchitecture in collagen scaffolds in *Chapter 2* (Fig 2.3b). Here, only collagen scaffolds were printed with the defined microarchitecture, and no B4F printing was performed in this stage.

Studies have revealed that endothelial cell migration enables the secretion of collagenase, which can lead to collagen degradation⁴⁶. This phenomenon was observed at about 10hr after endothelial cell seeding in our printed collagen scaffolds. Fig 3.1a shows the printed collagen scaffolds with seeded human umbilical-vein endothelial cells (HUVECs) at 0.5hr after seeding. At this moment, the printed collagen scaffolds preserved the original geometries. At 10hr after seeding, endothelial cells migrated and proliferated, and the degradation of printed collagen scaffolds occurred (Fig 3.1b). Endothelial cells also contracted and pulled the collagen scaffolds

to deform due the degradation of collagen scaffolds, leading to the failure of formation of microvasculature. In order to solve this problem, after acetic acid development and neutralization with PBS, the collagen scaffolds were crosslinked with glutaraldehyde, which is an extensive-used crosslinker in biochemistry applications. The glutaraldehyde crosslinking enabled stronger collagen scaffolds. The degradation of collagen scaffolds was reduced by this method.

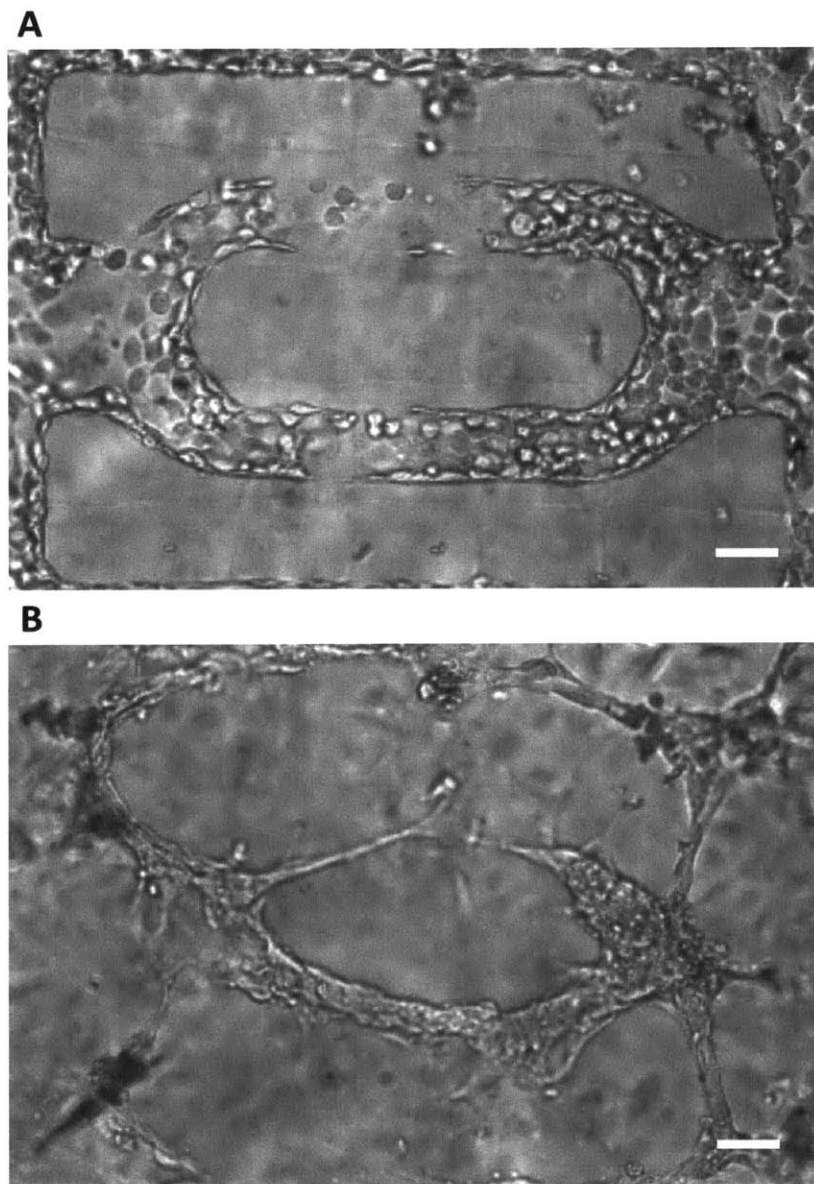


Fig 3.1: The degradation of printed collagen scaffolds. The printed collagen scaffolds (a) at 0.5hr and (b) at 10hr after seeding HUVECs

showed that the degradation of collagen occurred and HUVECs contracted and pulled the collagen scaffolds, leading to deformation of the microvasculature. Scalar bar = 50 μ m.

After glutaraldehyde crosslinking, the remaining glutaraldehyde was rinsed out and replaced with the culture media of HUVEC. HUVECs were then pipetted directly into the channel of the PDMS microfluidic device. Several trials of seeding were needed for making cells uniformly distributed (Fig 3.2a). After overnight incubation at 37°C, cells proliferated and migrated, adhering along the collagen walls and forming a densely packed monolayer of cells. The dual-capillaries of microvasculature was formed as shown in Fig 3.2b. The geometries of collagen scaffolds were kept well without degradation. Fig 3.3 shows the fixed and stained microvasculature at 12hr after seeding. Fig 3.3a shows VE-cadherin and Hoechst stains, and Fig 3.3b shows Phalloidin and Hoechst stains, imaged under epifluorescence microscopy. The cross-sectional views of A-A and B-B indicated a patent lumen within the microvasculature through which fluid could flow (Fig 3.3c), imaged under two-photon microscopy.

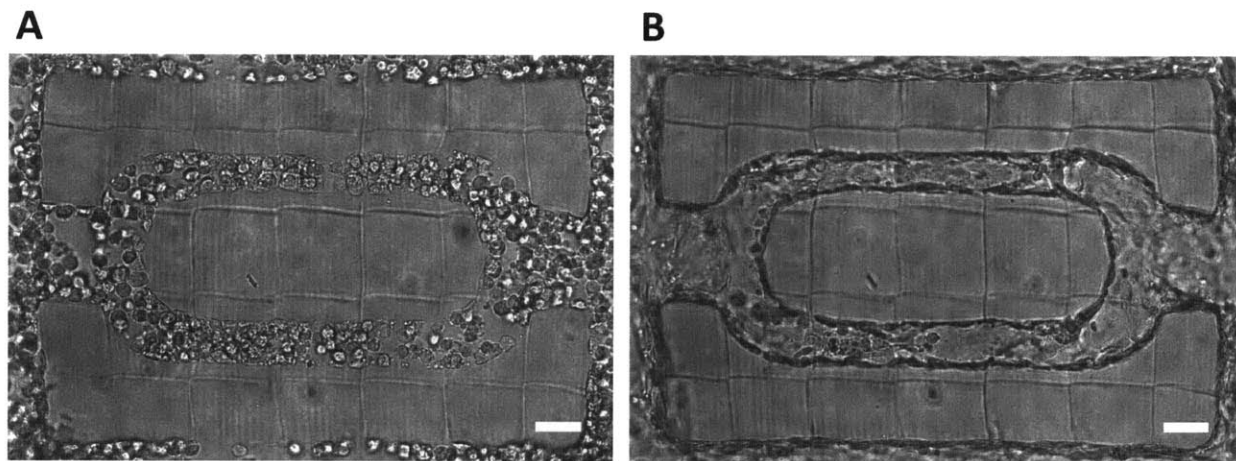


Fig 3.2: Microvasculature formation with glutaraldehyde crosslinking. (a) HUVECs were distributed uniformly after seeding. (b) At 12hr after HUVEC seeding, the microvasculature was formed with the densely packed monolayer of cells. Scalar bar = 50 μ m.

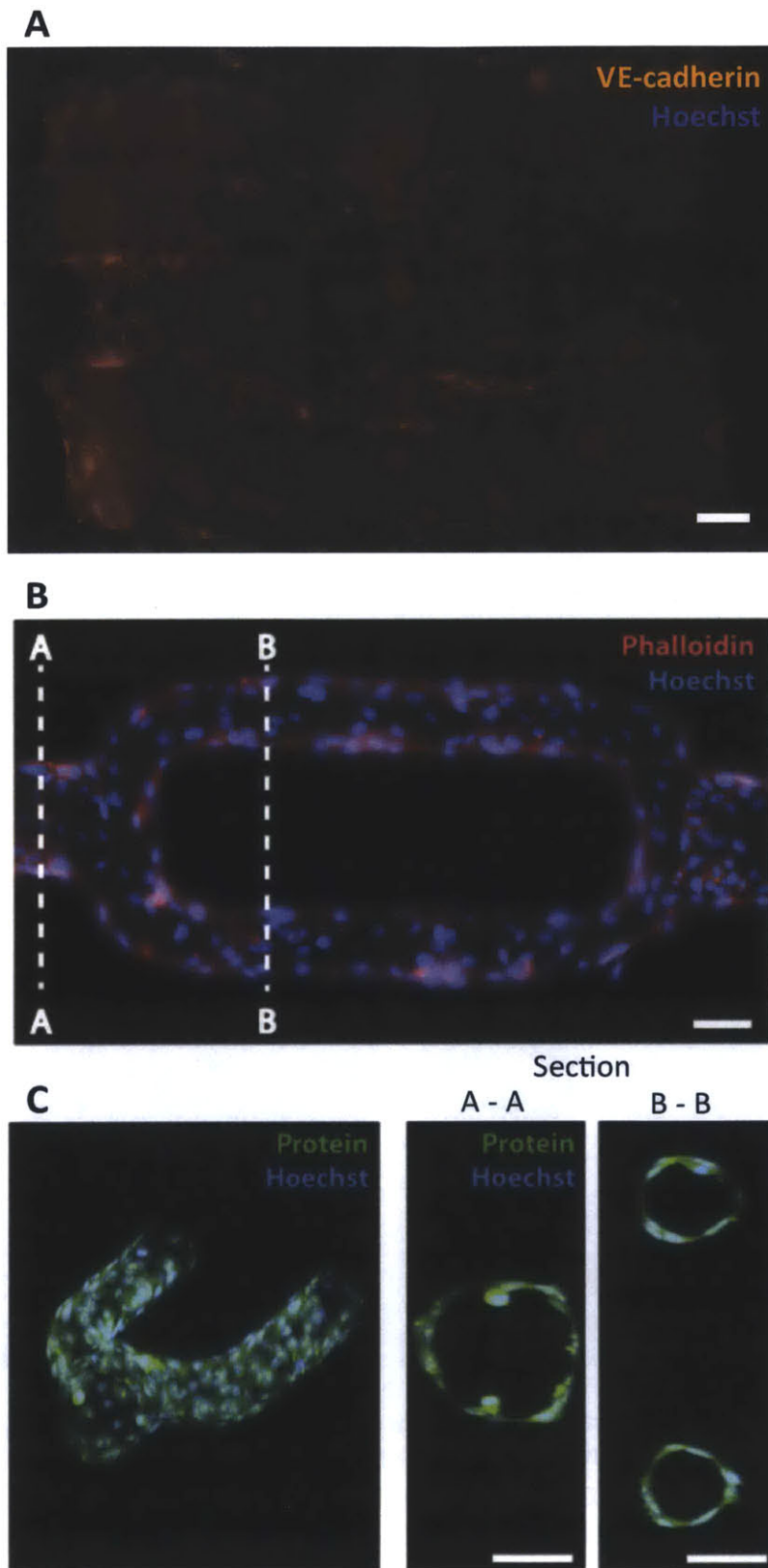


Fig 3.3: Microvasculature formation. The microvasculature at 12hr

after seeding was fixed and stained with (a) VE-cadherin and Hoechst staining, and (b) Phalloidin and Hoechst staining, imaged under epifluorescence microscopy, and (c) protein and Hoechst staining, imaged under two-photon microscopy. Scale bar = 50 μ m.

3.2.2 Schematic for leukocyte rolling in printed microvasculature

Fig 3.4 shows the schematic for leukocyte rolling in printed microvasculature. First, using the rapid 3-D laser microprinting technique, the structure of collagen scaffolds and internal patterns of streptavidin were printed the same as the structure in *Chapter 2* (Fig 3.4a). Here, we used biotinylated IL-1 or LPS for endothelial cell activation. Next, using the same HUVEC seeding method described in 3.2.1, the microvasculature was formed (Fig 3.4b). The leukocyte rolling assay was conducted at 16 or 22hr after HUVEC seeding (Fig 3.4c). During this period of time, cells were proliferated and migrated to form the vasculature, and also the activation of IL-1 or LPS occurred on the vascular wall.

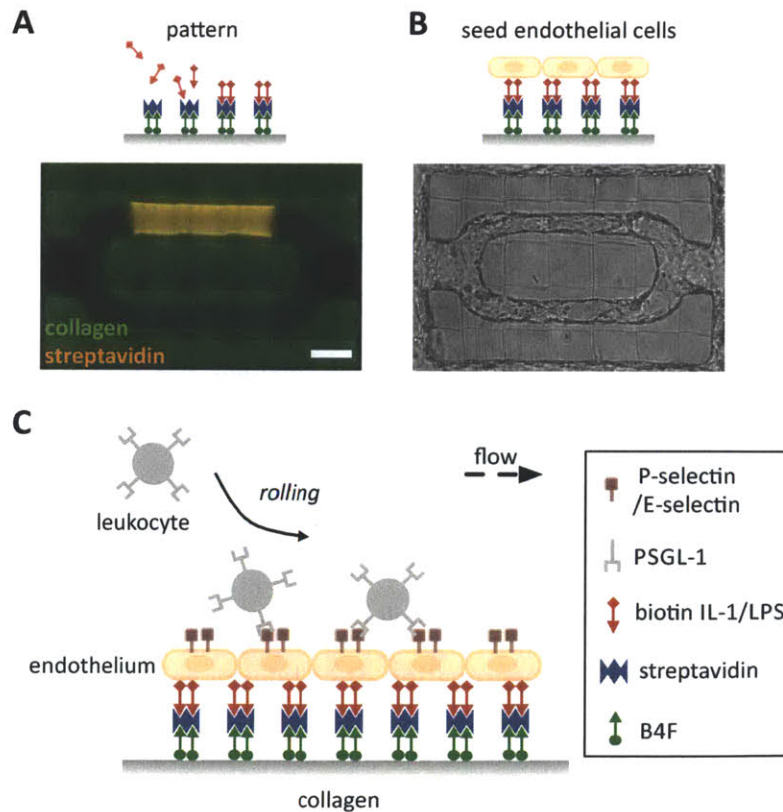


Fig 3.4: Schematic for leukocyte rolling in printed microvasculature.

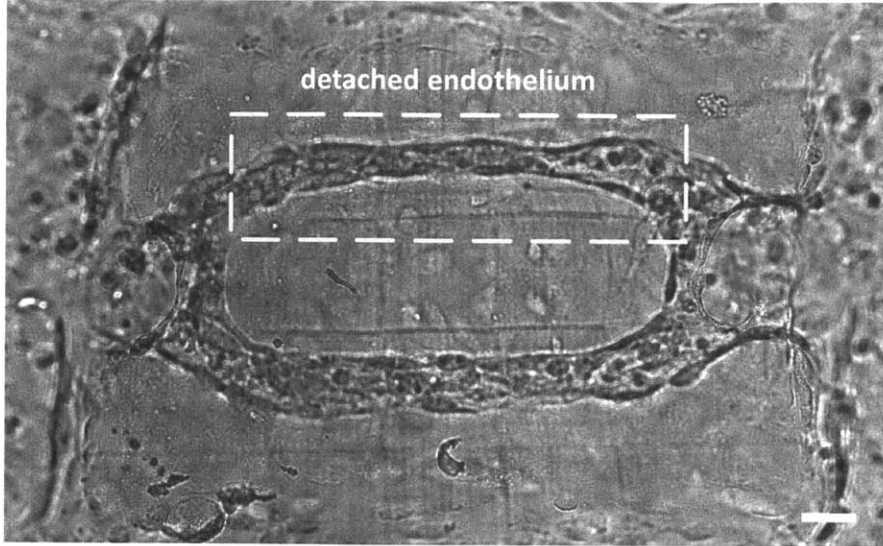
(a) The microstructure of collagen scaffolds and the internal protein patterns were first printed, and (b) HUVECs were seeded to form the microvasculature. (c) Leukocyte rolling assay could be conducted within the microvasculature.

3.2.3 Improvement in formation of microvasculature

Fig 3.5a shows the detached endothelium occurred on the IL-1/LPS patterned collagen channel, while the endothelial cells on the unpatterned collagen channel adhered well to the collagen wall. We hypothesized the cause might be the lack of binding sites for HUVECs on collagen which were mostly taken by patterned B4F, streptavidin, and biotinylated IL-1/LPS. The detached endothelium led to a narrower and unhealthier capillary, so the leukocytes might be unable to flow through the narrow capillary or the results of leukocyte rolling assay might not be convincing because of the unhealthier capillary. In order to solve this problem, fibronectin, an extracellular protein widely used for cell adhesion, was added to coat onto the collagen wall right before the HUVEC seeding. This method worked very well. The fibronectin coating provided more binding sites for HUVECs on patterned collagen wall. The endothelium on the patterned collagen channel adhered well to the collagen wall just as on the unpatterned collagen channel.

Fig 3.5b shows cell debris aggregated in the microvasculature. This phenomenon occurred frequently during the period that HUVECs formed the vasculature. The cell debris would block the channels, and leukocytes could not be flowed through the vasculature, leading to the failure of leukocyte rolling assay. To remove the cell debris during the period of formation of vasculature, a syringe pump was used to draw the liquid out of one well in microfluidic device, and a flow of fresh culture media from the other well would be driven through the vasculature by the pressure drop. Using this method, the cell debris had chance to be brought away by the flow. This method worked well. The aggregation of cell debris in the vasculature was reduced, and the vasculature seemed to be healthier.

A



B

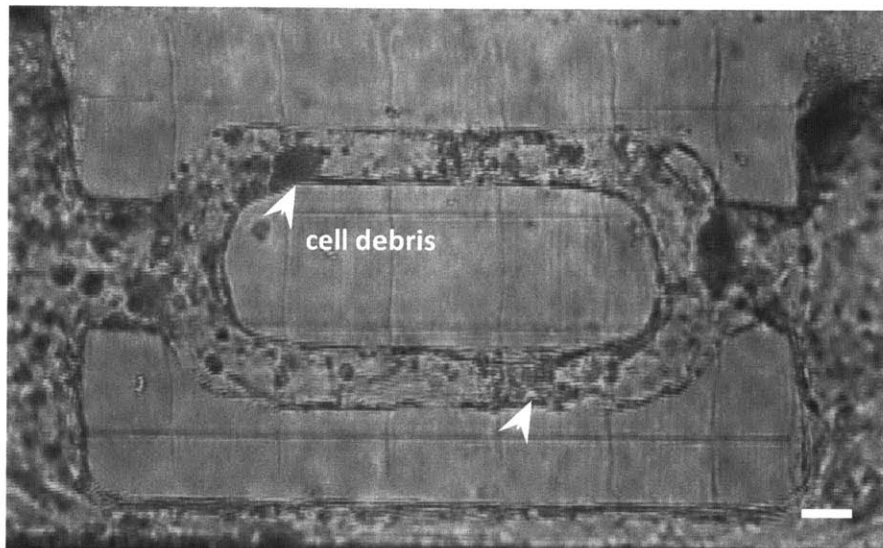


Fig 3.5: Improvement in formation of microvasculature. (a) The detached endothelium occurred because of the lack of binding sites in patterned collagen channels, and this problem could be solved by coating of fibronectin. (b) Cell debris blocked the collagen channels, and this problem could be reduced by creating continuous flow through the channels overnight. Scale bar = 50 μ m.

3.2.4 HL-60 leukocyte rolling assay within printed microvasculature

When the printed microvasculature was at 16 or 22hr after seeding, HL-60 leukocyte rolling assay was conducted using the same method in *Chapter 2*. The results of HL-60 leukocyte rolling assay in printed microvasculature were not quantified due to the limit number of experiments and the unclear images. However, by eye observation, the results of HL-60 leukocyte rolling assay could still be determined. Cells were counted as rolling if their speeds were much slower compared to the flow rate, which was the non-rolling cell flow speed. At 16hr after seeding, HL-60 cell rolling on endothelium occurred on both LPS patterned and unpatterned collagen channels, but the cell rolling numbers and ratio were very low. At 22hr after seeding, HL-60 cell rolling on endothelium also occurred on both LPS patterned and unpatterned collagen channels (Fig 3.6), and the cell rolling number and ratio were much higher than at 16hr. For IL-1 activation, the results were the same as LPS activation. HL-60 cell rolling on endothelium occurred on both IL-1 patterned and unpatterned collagen channels at 16hr and 22hr, and more cells rolled at 22hr. In addition, the cell rolling numbers and ratio of IL-1 activation seemed to be lower than LPS activation.

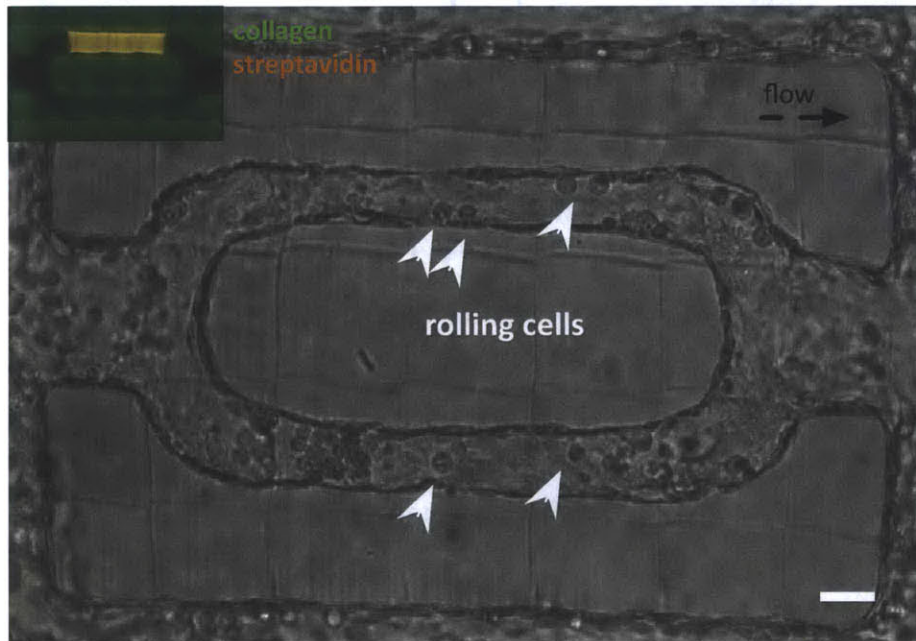


Fig 3.6: Leukocyte rolling assay within printed microvasculature. The HL-60 leukocyte rolling occurred on both patterned (up channel)

and unpatterned (down channel) collagen channels. Scale bar = 50 μ m.

One positive control and one negative control experiment were conducted to further prove that HL-60 cell rolling on endothelium was due to the activation of printed protein patterns. The negative control experiment was conducted in a printed collagen scaffolds without B4F printing. After 12hr of microvasculature formation, HL-60 leukocytes were flowed through the printed collagen channels without B4F printing. No HL-60 rolling occurred in both collagen channels. After the negative control experiment, the same microfluidic chip was used for the positive control experiment. The soluble LPS was added into the chip for 4hr activation on endothelium. After 4hr of activation, HL-60 leukocytes were flowed into the chip for positive control experiment, and HL-60 cell rolling occurred on both collagen channels.

3.3 Discussion

The printed microvasculature was formed by HUVECs seeded into the printed collagen scaffolds. Phalloidin staining showed the clear F-actin filaments in HUVECs; VE-cadherin staining showed the cell-to-cell adhesions in microvasculature; and the cross-sectional views of microvasculature showed the hollow capillaries. They verified a successful formation of microvasculature using the rapid 3-D laser microprinting technique. Also, the 3-D printed collagen scaffolds were proved to be biocompatible. To further study the properties and functions of printed protein patterns from rapid 3-D laser microprinting, leukocyte rolling assay was performed within the printed microvasculature. Endothelial cells of microvasculature were activated by printed IL-1 or LPS, and after activation, HL-60 cell rolling occurred on both patterned and unpatterned collagen channels. Moreover, HL-60 cells didn't roll in negative control experiments, and HL-60 cells rolled on both collagen channels in positive control experiments.

Here, we can have some possible conclusions. First, the results from the negative and positive control experiments indicated that the printed microvasculature was activated by soluble LPS and so HL-60 cells rolled on the activated endothelium. Second, HL-60 cell rolling occurred on

both LPS/IL-1 patterned and unpatterned collagen channel, and this result could be concluded that the printed LPS/IL-1 functioned and activated the endothelial cells in microvasculature. Third, we hypothesized that the activated endothelial cells might express signals to their nearby cells, so the endothelial cells on patterned and unpatterned channels are all activated. In this dimension of microvasculature, the activation of endothelium might not be a local effect of printed proteins.

The evidence for the possible conclusions above was still not convincing enough. The LPS/IL-1 activation on endothelium was not well proved. The activation might be caused by other factors, such as the printed streptavidin. There were only limited numbers of experiments (N=3) that the results observed here might be coincidence. Also, the results were not quantified, and this problem can be improved by taking videos and images of leukocyte rolling assay with higher resolution or labeling the HL-60 leukocytes with fluorescence or dye. To sum up, the leukocyte rolling experiments in printed microvasculature needs more in improvement. However, we still learned much from these results. First, we could summarize that the printed proteins using rapid 3-D laser microprinting technique functioned and activated the seeded endothelial cells. Second, the seeded endothelial cells formed a microvasculature, which preserved endothelial cells' function and verified the biocompatibility of printed collagen scaffolds. Last, the rapid 3-D laser microprinting technique may be utilized in determining a local effect of printed proteins in the future.

3.4 Conclusion

We have demonstrated a 3-D printed microvasculature, which was formed successfully using the rapid 3-D laser microprinting technique. The leukocyte rolling assay performed in the printed microvasculature showed that the printed proteins preserved their functions and properties, and the printed collagen scaffolds were biocompatible. Moreover, one potential application of the rapid 3-D laser microprinting may be the examination of a local effect of printed proteins.

3.5 Detailed Methods

3.5.1 Cell culture

Human umbilical-vein endothelial cells (HUVECs) were obtained from Lonza (Basel, Switzerland) and cultured in Endothelial Basal Media supplemented with an EGM-2 Bulletkit (Lonza) in an incubator at 37 °C with 5% CO₂. HUVECs were passaged with tryPLE (Life Technologies). HUVECs of passage number 4 to 8 were used in all experiments. HL-60 cell culture was described in 3.5.4.

3.5.2 Formation of microvasculature

The fabrication of PDMS microfluidic chips was described in 2.5.1. The collagen scaffolds preparation was described in 2.5.2. The printing of collagen scaffolds was described in 2.5.3. 0.6% v/v glutaraldehyde (Sigma-Aldrich, St. Louis, MO) in DI water was used for crosslinking the collagen scaffolds for 10 minutes. The biotinylated IL-1 and LPS were used at 10 µg/ml in 3% BSA (IL1 and LPS, InvivoGen, San Diego, CA). After the addition of biotinylated IL-1/LPS in the microfluidic chip, the unbound IL-1/LPS was rinsed out with PBS and replaced with 10 µg/ml of fibronectin (EMD Millipore, Billerica, MA) in DPBS for coating onto the collagen channel walls. After 30 minutes of fibronectin coating, the remaining fibronectin was rinsed out and replaced with HUVEC cell culture media. 2µl of HUVECs were then seeded into the collagen scaffolds. Several trials of seeding were taken until cells were distributed uniformly. At one hour after seeding, HUVECs were attached to the collagen channel walls, and one well of the microfluidic device was pumped out the culture media at a rate of 0.3µl/min. The syringe pump and the microfluidic device were put in the incubator at 37 °C. By using this method, the flow was helped to remove cell debris in the collagen channels and keep the seeded cells healthier.

3.5.3 Staining of microvasculature

After the 12hr of formation of microvasculature, cells were fixed in 4% paraformaldehyde for 10 minutes. The cells were permeabilized for 3 minutes in 0.1% Triton X-100, and blocked in 1%

casein for 30 minutes. F-actin filaments were labeled by incubation with 2 U/ml phalloidin-Alexa Flour 594 (Life Technologies) in 1% casein for 30 minutes. VE-cadherin were stained by incubation with VE-cadherin-Alexa Flour 488 (Life Technologies) in 1% casein for 1hr. Nuclei were stained by a 3 minute incubation in 1:5000 Hoescht solution. To obtain a bright staining for high-contrast two photon imaging of 3-D microvasculature, cellular protein was stained by adding 50 $\mu\text{g}/\text{ml}$ of Alexa Flour 488-NHS (Thermo Scientific) in PBS through the collagen channels for 5 minutes, followed by rinses in PBS.

3.5.4 Leukocyte rolling assay

When the printed microvasculature was ready for leukocyte rolling experiments, the microfluidic chip was first equilibrated with the HUVEC cell culture media, and 2 μl of HL-60 cells were added to one well to drive a flow of cells through the channels. For consistency of flowing profile, this process was used in every rolling experiment. For the positive control experiments, the printed microvasculature was incubated with 10 $\mu\text{g}/\text{ml}$ of LPS in HUVEC culture media for 4hr of endothelial cell activation.

3.5.5 Image and data analysis

The two-photon images were taken by a two-photon fluorescence microscope (Prairie Technologies, Middleton, WI) using a MAI-TAI laser.

Videos were taken under microscope during HL-60 leukocyte rolling experiments. The rolling of cells was determined by eye observation.

Chapter 4: GUIDING AND HOMING OF CELLS IN 3-D MICROPRINTED COLLAGEN SCAFFOLDS

In this chapter, we demonstrate a 3-D microprinted collagen scaffolds for guiding and homing of cells developed by the rapid 3-D laser microprinting technique. We introduce the cycle of innovation for achieving the goals. The rapidly prototyping process can be achieved by the rapid 3-D laser microprinting technique. We also prove that the combination of microstructures and internal protein patterns in collagen scaffolds is necessary for guiding and homing of cells in 3-D microprinted collagen scaffolds.

4.1 Background and Motivation

4.1.1 Artificial stem cell niche in regenerative medicine

Stem cells are defined by their ability to self-renew and specialize, so they are critical for the regeneration of aged, injured and diseased tissues⁴⁷. Stem cell niche is a complex, multifactorial local microenvironment, which interacts with stem cell to regulate cell fate, consisting of stem cells, non-stem cells, an extracellular matrix and molecular signals⁴⁸. The niche provides both anatomic and functional dimensions for stem cells to present their ability to self-renew and specialize, and without the niche, stem cells generally have limited functions⁴⁹. The cellular interaction between stem cells and niche cells, the engagement of stem cells with the extracellular matrix, and the soluble and immobilized signaling factors within the stem cell niche lead to the complexity of the stem cell niche⁵⁰. The schematic depiction of the stem cell niche is shown in Fig 4.1.

Artificial stem cell niche is promising in exploiting the unique self-renewal and differentiation potential of stem cells in regenerative medicine⁵¹. Researchers have studied on generating the cell culture platform with the functions and structural microenvironments of the stem cell niche. Lutolf and Blau have reviewed the recent methods of generating the artificial stem cell niches, including the use biomolecular materials with niche-like characteristics, the protein microarrays to dissect niche complexity, mimicking the spatial complexity of niche signals, and rebuilding

complex tissue-like structure via 3-D bioprinting approaches⁵¹. The methods for creating artificial stem cell niches are thought to be promising for stem cells used in clinics and as a diagnostic tool⁵².

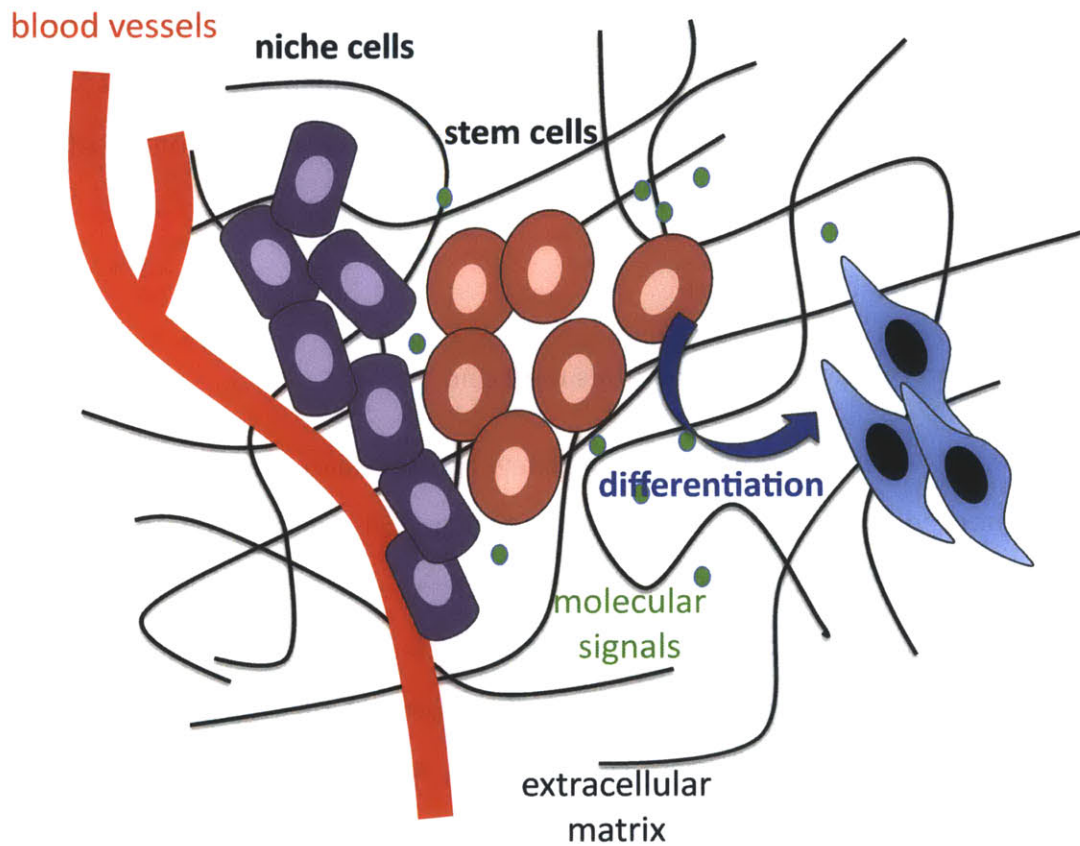


Fig 4.1: The schematic depiction of stem cell niche. The stem cell niche consists of stem cells, niche cells, blood vessels, molecular signals and extracellular matrix. Image adapted from Vazin and Schaffer⁵⁰.

4.1.2 Guiding and homing of cells: the first step to create an artificial stem cell niche using rapid 3-D laser microprinting

Here, we proposed that the rapid 3-D laser microprinting might be a potential tool for generating the artificial stem cell niche. Stem cell niches are known as its complexity of functionality, structures and compositions in a microenvironment. The advantage of the rapid

3-D laser microprinting method is the capability of creating defined 3-D microarchitectures of scaffold materials and printing desired 3-D patterns of protein cues inside scaffolds, and this advantage might generate an in-vitro microenvironment for the stem cell niche, which consists of many cell types, molecular signals and blood vessels in extracellular matrix (Fig 4.1). In order to create the microenvironment of stem cell niches, we would like to start from achieving guiding and homing of cells to specific locations inside scaffolds. This first step allowed the future work for guiding and homing of multiple cell types inside scaffolds to create the artificial stem cell niches.

The idea of guiding and homing of cells was from the leukocyte rolling assay describe in *Chapter 2*. We utilized the binding of PSGL-1 and P-selectin ligands for catching cells and then directing them into a trap. In this chapter, we only demonstrated the guiding and homing of HL-60 leukocytes. However, the guiding and homing of stem cells could be achieved by gene transfection of stem cells to express PSGL-1 and enable stem cell rolling. In addition, after achieving stem cell homing, we can incorporate the method described in *Chapter 3* to grow blood vessels near the stem cells, and a simple model of artificial stem cell niche can be created.

4.2 Results

4.2.1 Schematic for guiding and homing of cells

The results of cell rolling described in *Chapter 2* gave the idea of catching and guiding of cells. When leukocytes were flowed through the collagen channels with printed P-selectin patterns, the fast-moving cells were caught by the printed P-selectin patterns due to PSGL-1 and P-selectin binding. As we discussed in *Chapter 2*, once the cells touched the P-selectin patterned collagen walls, they would start to roll. This phenomenon could be utilized to catch and guide the cells. In order to accumulate the caught cells in a specific location, a “trap” was designed to let the caught cells to be stored, and so the homing of cells could be achieved.

Fig 4.2a shows the concept of guiding and homing of cells. A “runway” collagen channel of

printed P-selectin patterns catches cells from a flow and directs them into a trap. The bulge-shape trap is also patterned with printed P-selectin, and it allows cells to be guided from the runway to the trap and then be accumulated in the trap. We termed this design as “runway-traps”. Fig 4.2b shows the control group for the experiments. No P-selectin patterns are printed in the runway-traps. Cells don’t have chance to be caught, so they will just flow through the collagen channel without being trapped. The control group helps to prove the combination of printed collagen scaffolds and internal protein patterns is necessary for achieving the guiding and homing of cells.

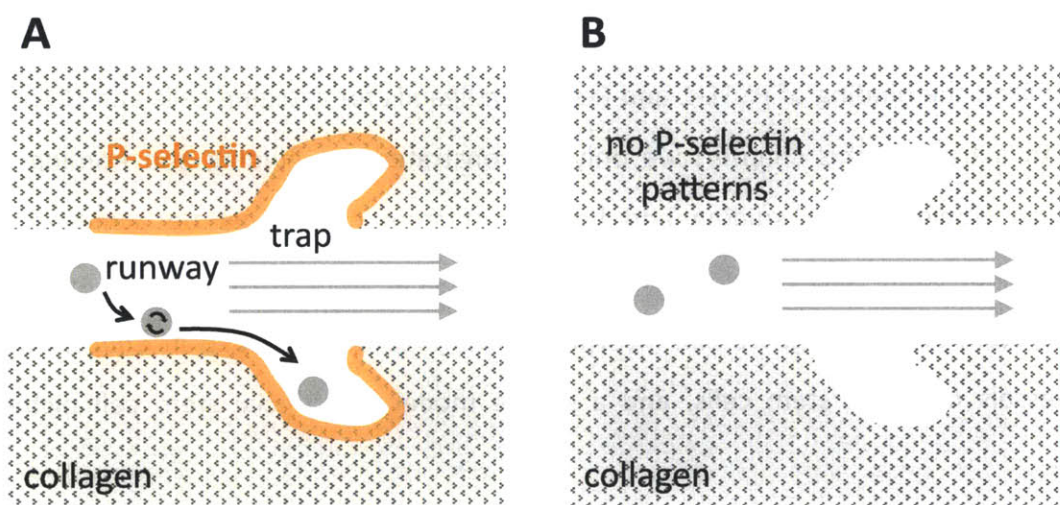


Fig 4.2: Schematic of guiding and homing of cells. (a) The P-selectin patterned runway catches cells and guides them into a trap. (b) The control group has the same geometries but without P-selectin patterns, so cells don’t have chance to be caught and trapped.

To create the collagen scaffolds microstructure for guiding and homing of cells, we used the same design of the PDMS microfluidic device in *Chapter 2* and *Chapter 3* (Fig 2.3a), which contained the collagen scaffolds for printing and allowed to drive a flow within the collagen scaffolds for cell flowing through. Fig 4.3 shows the collagen scaffold microstructure, which consisted of two identical branched channels. The branched collagen channel consisted of a runway with a diameter of 50 μ m and a bulge-shape trap. The size of whole microstructure was 700 \times 500 \times 150 μ m (length \times width \times height) printed in 5 rows and 7 columns of 100 \times 100 \times

150 μm sections. One of branched channels was printed with an annular pattern of P-selectin, which was designed with an inner diameter of 4 μm smaller than the collagen channel diameter and with an outer diameter of 6 μm larger than the collagen channel diameter to ensure P-selectin ligands were printed on the surface of collagen channels. The patterned branched channel is leukocyte rolling and trapping zone, and the unpatterned branched channel is the control zone.

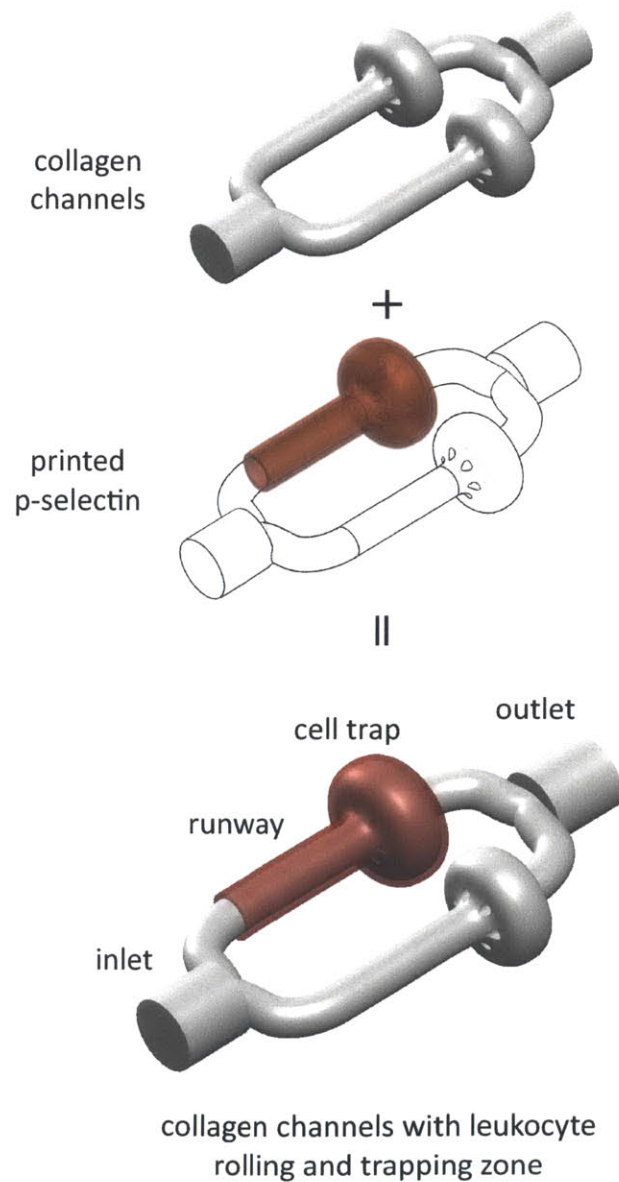


Fig 4.3: The microstructure of collagen scaffolds. The branched collagen channel consisted of a runway with a diameter of 50 μm and

a bulge-shape trap. One of branched channels was printed with an annular pattern of P-selectin. The patterned branched channel is leukocyte rolling and trapping zone, and the unpatterned branched channel is the control zone.

4.2.2 Cycle of innovation

Numerous iterative designs of the runway-traps were generated in order to find a successful one. This rapid prototyping process could be easily achieved by the rapid 3-D laser microprinting technique. First, we designed a 3D model of collagen channels and P-selectin patterns using *SolidWorks* (as described in *Chapter 1*). Next, the 3D model was printed in the collagen scaffolds and P-selectin ligands were patterned using the rapid 3-D laser microprinting method. After that, HL-60 leukocytes were flowed through the printed collagen scaffolds, and the performance could be then assessed. After HL-60 cells flowed through the collagen channels and trapped in the bulges, the excess cells were rinsed out by pipetting in the two wells of the microfluidic device. After rinsing, the cell numbers trapped in the bulge were counted by eye observation. By assessing the performance of the design, we could then design the next generation of 3D model, and this cycle of innovation was repeated until a successful design was determined (Fig 4.4).

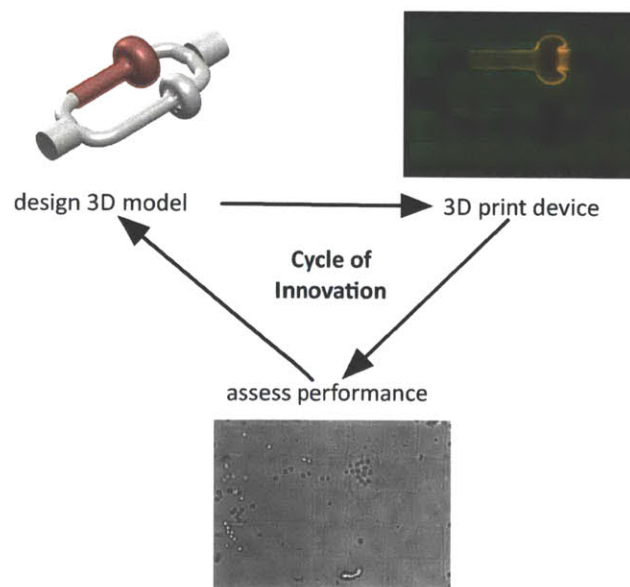


Fig 4.4: The cycle of innovation. First, we designed the 3D model of collagen channels and P-selectin patterns. Second, we printed the

3D model using the rapid 3-D laser microprinting technique. Next, by assessing the performance by flowing HL-60 cells through the printed collagen scaffolds, we could design the next generation of 3D model.

4.2.3 Design evolution

Fig 4.5 shows the first generation of design. The trap was designed to be a sphere-like bulge, and placed in the middle of the branched channel. The P-selectin patterns were printed on the half of collagen channel and the sphere-like trap. After HL-60 cells flowed through the collagen channels, few cells rolled on the patterned runway and no cells were trapped in the sphere-like bulge. In the unpatterned collagen channel, no HL-60 cell rolling occurred and cells just passed through the channel. The performance of the first design indicated that the runway was too short to catch enough cells to roll on, and cells could not be guided into the bulge.

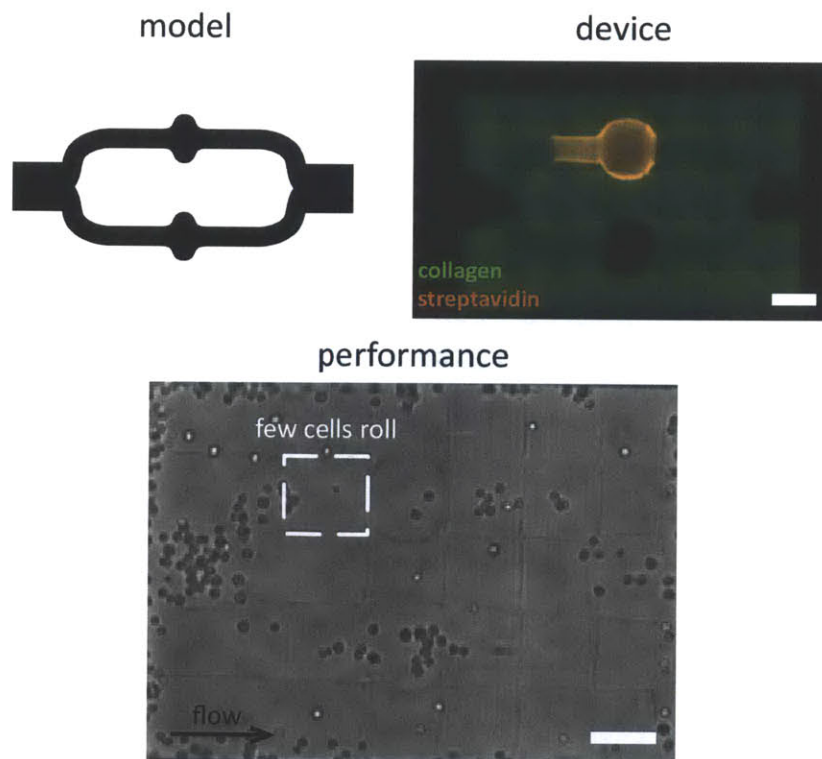


Fig 4.5: The first generation of design. There were few cells rolling on P-selectin patterned runway because of the insufficient length. Scale bar = 100 μ m.

Fig 4.6 shows the second generation of design. The second generation of design improved the problems in the first design. The runway was lengthened to catch more cells, and the corner between the runway and the bulge was steeper. The P-selectin patterns were printed on the lengthened runway and the bulge. After HL-60 cells flowed through the collagen channels, there were much more cells rolling on the patterned runway, and the rolling cells were directed into the bulge. However, cells rolled into the bulge and then rolled out of the bulge. There was no trapped cell. In the unpatterned collagen channel, no HL-60 cell rolling occurred and cells just passed through the channel. The performance of the second design showed that the shape of the bulge needed to be improved.

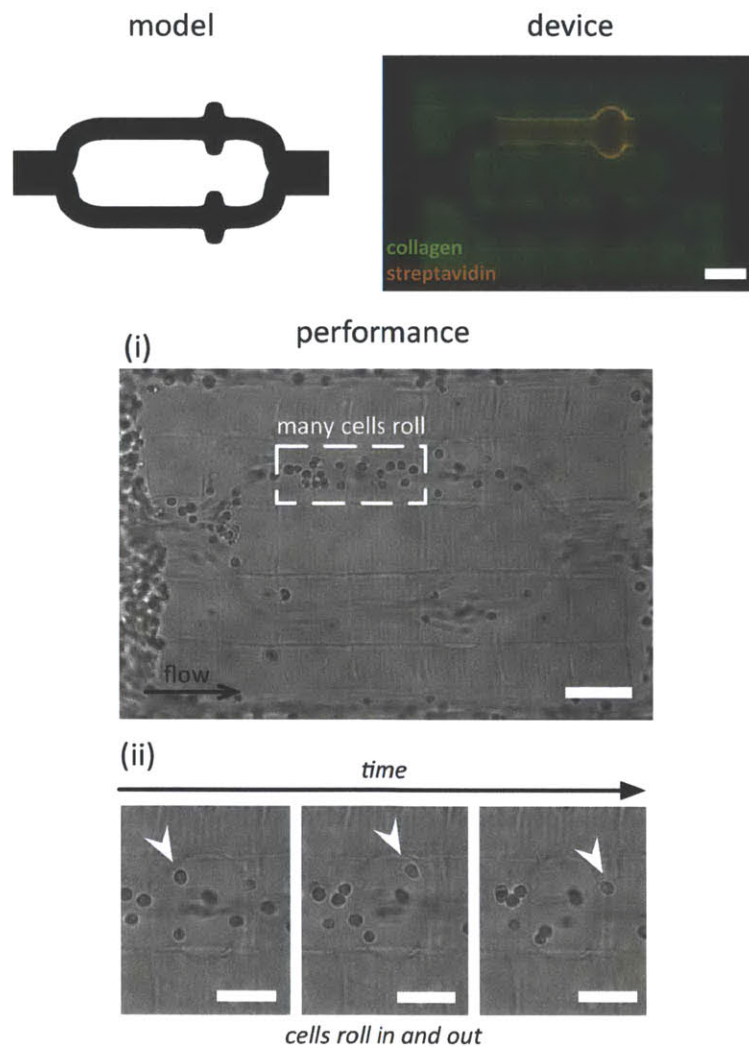


Fig 4.6: The second generation of design. (i) Many cells roll on the

lengthened runway, and cells were caught and directed into the bulge-like trap. (ii) The trap was unable to restore the cells, since cells just rolled in and rolled out of the trap. Scale bar = 100 μ m, except the scale bar in (ii) = 50 μ m.

Fig 4.7 shows the third generation of design. In the third generation of design, we added the overhangs in the bulges, so the rolling cells could roll into the bulges, but they were not allowed to roll out of them. The P-selectin patterns were still printed on the long runway and the bulge with overhangs. After the printing of collagen scaffolds, the geometries of bulges were not shown the same as our 3D model design. The printed bulges didn't have the overhanging flaps. Thinking in three dimensions, the overhangs were thin and not supported, so they were easily blown away by the flow, leading to the inverted overhangs. The inverted overhangs could be observed under the microscope. Therefore, after flowing HL-60 cells through the collagen channel, many cells rolled on the patterned runway and then still rolled in and rolled out of the bulges. In the control group of collagen channel, no HL-60 cell rolling occurred and cells just passed through the channel.

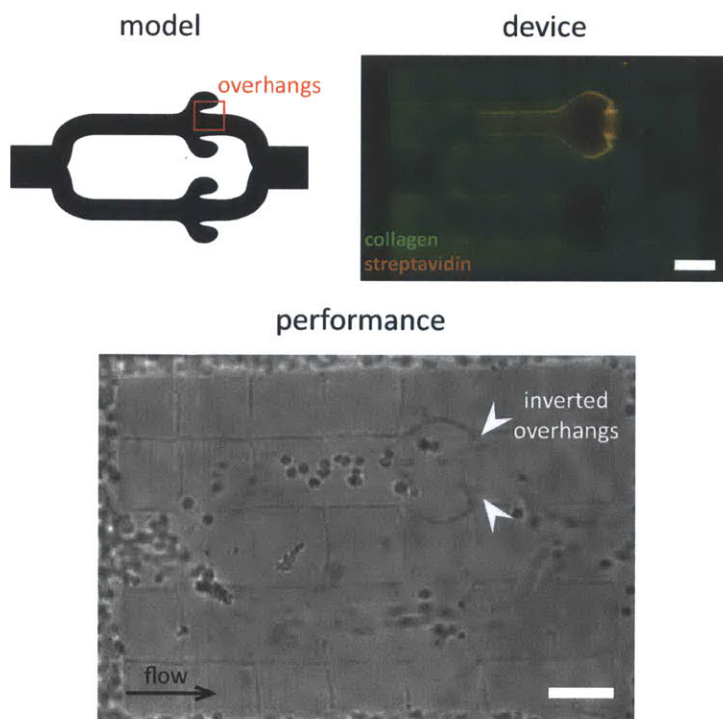


Fig 4.7: The third generation of design. We added the overhangs to

trap cells in the bulges. However, the overhangs were too thin and without supports, so they flapped by the flow in the channels, leading to the inverted overhangs. Scale bar = 100 μ m.

In order to solve the problem of inverted overhangs, we designed the collagen tethers to support the overhangs in the bulges (Fig 4.8a). The hollow tube pointed in Fig 4.8a was the collagen tether, which held the overhangs with the collagen scaffolds. We designed six collagen tethers with a diameter of 15 μ m to support the overhangs, because too many tethers would block the cells to roll into the bulges. The two-photon images in Fig 4.8b, c and d show the printed collagen scaffolds with improved bulge design. Fig 4.8c shows the clear view of two collagen tethers, which supported the overhangs and made the bulge in desired shape. Fig 4.8d shows the cross-sectional view of B-B, and six collagen tethers were distributed in the bulges.

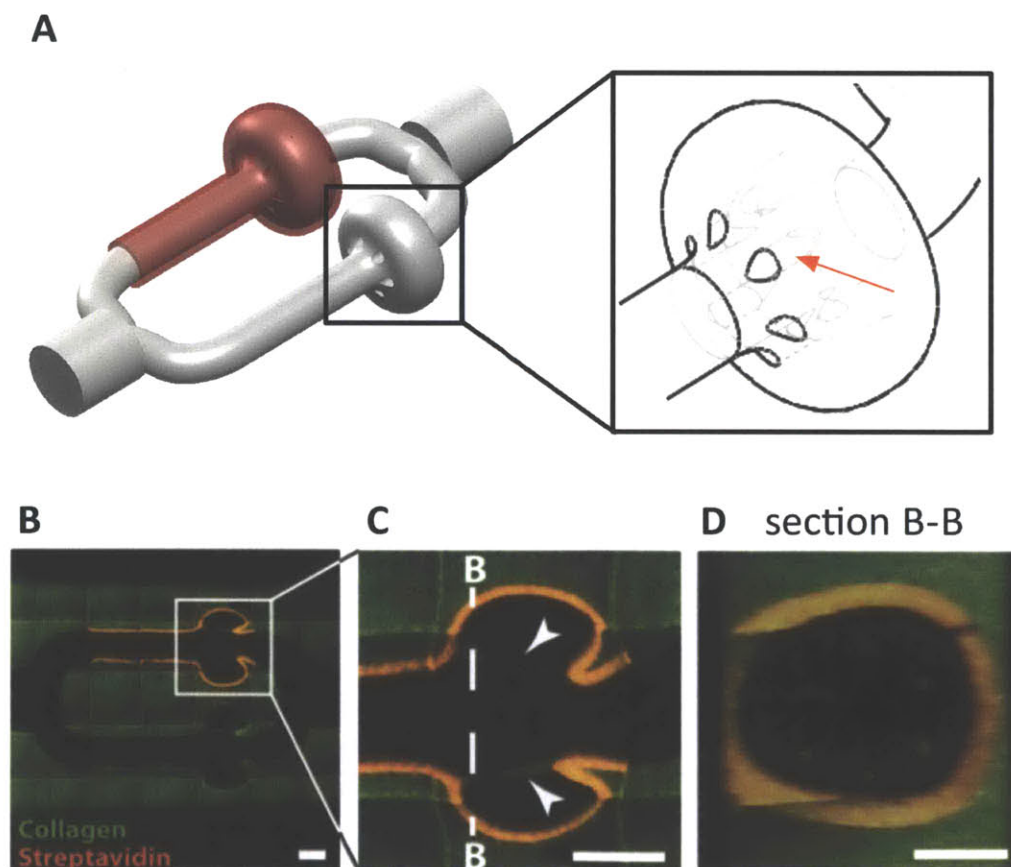


Fig 4.8: The tether design. Six collagen tethers with a diameter of 15 μ m were designed to support the overhangs. The geometries of bulges were kept in desired shape. Scale bar = 50 μ m.

Fig 4.9 shows the fourth generation of design, and it's also the final one. As mentioned above, we added six collagen tethers to support the overhangs and keep the bulges in desired shape. After flowing HL-60 cells, the rolling cells on the patterned runway were directed into the bulges and then trapped by the bulges. Part of rolling cells still rolled out of the bulges, but part of rolling cells were trapped. In the unpatterned collagen channel, no HL-60 cell rolling occurred and cells just passed through the channel. After washing out the excess HL-60 cells, there were about 20 cells trapped in the patterned bulge.

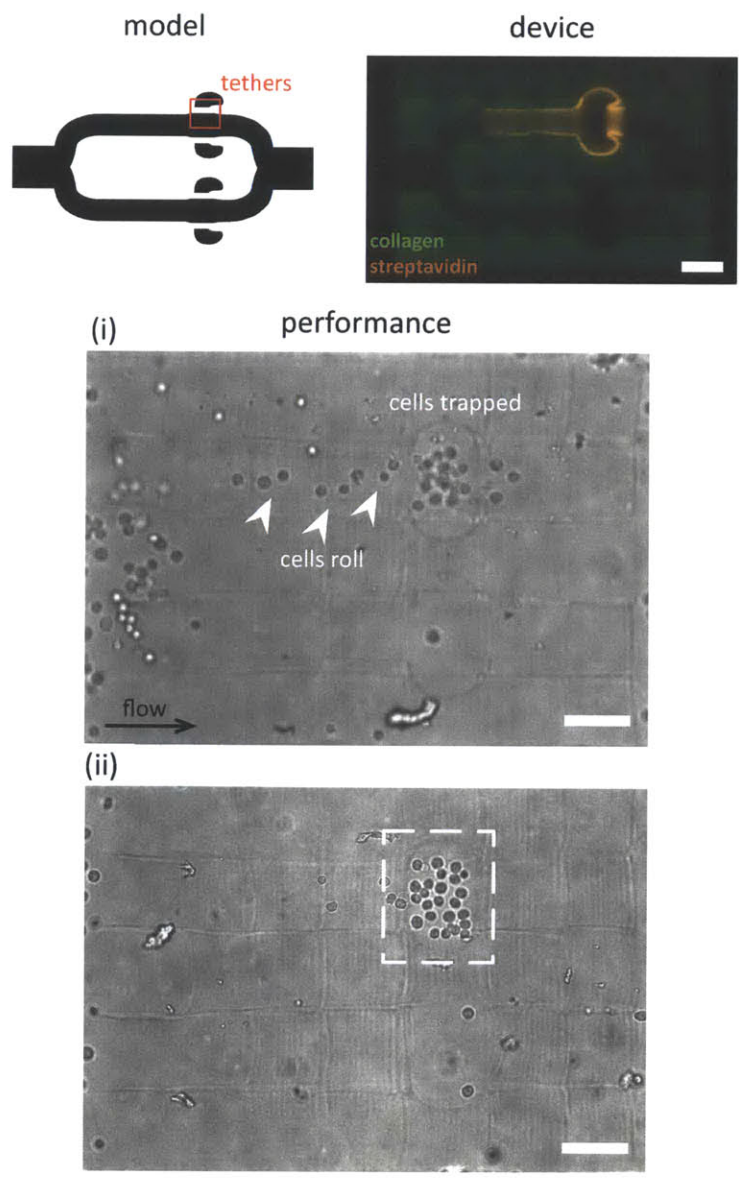


Fig 4.9: The fourth generation of design. The improved bulge with

collagen tethers was able to trap the rolling cells. After washing out the excess cells, the patterned bulge trapped about 20 cells, while the unpatterned bulge trapped no cells. Scale bar = 100 μ m.

4.3 Discussion

The summary of the four generations of design is shown in Table 4.1. For each generation, we designed the 3D model, printed the 3D model in the collagen scaffolds and patterned P-selectin ligands, assessed the performance by flowing HL-60 leukocytes, and then designed the next generation of 3D model that improved the previous one. In the end of this cycle of innovation, we lengthened the runway to catch more cells to roll; we added overhangs in the bulges to trap cells; and we created collagen tethers to support the overhangs. After flowing HL-60 leukocytes, cell rolling occurred on the P-selectin patterned runways, and then rolling cells were directed into the bulges and trapped by the overhangs. The last generation of design successfully achieved the guiding and homing of cells.





Design	Improvement	Performance
	Original design	Insufficient runway length that few cells roll.
	Lengthen runways to catch more cells	Many cells roll in the runway but cells just roll in and out of the bulge.
	Add overhangs to trap cells	Inverted overhangs that cells still roll in and out of the bulge.
	Add collagen tethers to support overhangs	Overhangs are supported by the collagen tethers, and cells are trapped.

Table 4.1: The summary of four generations of design.

For the last generation of design, when HL-60 leukocytes rolling through the collagen scaffolds, there was no cells rolling on unpatterned collagen channel and so no cells were directed into the bulges. However, sometimes cells would stick to the collagen wall of the bulges, and those stuck cells would stick more cells. Nevertheless, when we pipetted out the excess cells, those stuck cells would be rinsed out by the turbulent flow of pipetting, and only trapped cells would be left in the bulges. This rinsing gave a strong turbulent flow within the collagen channels, and it proved that cells were truly trapped and stored in the P-selectin patterned bulges. On the other hand, the geometries of unpatterned collagen channels were the same as the P-selectin patterned channel, and only the patterned channel trapped HL-60 cells. We can conclude that the combination of printed protein patterns and printed microstructures was necessary for achieving the guiding and homing of cells, and the rapid 3-D laser microprinting technique allows to print the combination of microarchitectures and internal protein patterns.

The cycle of innovation showed the importance of rapid prototyping, which is a widely used process for product design and manufacturing. Using rapid 3-D laser microprinting, we could rapidly prototype numerous iterative designs to achieve our goals. In addition, the microstructures in collagen scaffolds of the final design were in complex and high-resolution required geometries (e.g. the collagen tethers with a diameter of 15 μ m), and these complex and arbitrary microstructures in high-resolution could be easily achieved by the rapid 3-D laser microprinting method.

4.4 Conclusion

We have demonstrated a printed collagen scaffolds with complex geometries and internal proteins patterns for guiding and homing of cells. Multiple, iterative designs were generated to achieve the goals, and the rapid 3-D laser microprinting allowed this rapidly prototyping process. In the final design, a microstructure of collagen scaffolds successfully trapped about 20 cells in the patterned bulge. The combination of microarchitectures and internal protein patterns in collagen scaffolds was proved to be necessary for achieving the guiding and homing of cells.

4.5 Detailed Methods

4.5.1 Preparation of 3-D microprinted collagen scaffolds for guiding and homing of cells

The preparation of 3-D microprinted collagen scaffolds for guiding and homing of cells was the same as *Chapter 2*. The fabrication of PDMS microfluidic chips was described in 2.5.1. The collagen scaffolds preparation was described in 2.5.2. The printing of collagen scaffolds was described in 2.5.3. The HL-60 leukocytes were prepared as described in 2.5.4.

4.5.2 Experiment for guiding and homing of cells

When the microfluidic chip was ready for experiments, the collagen channels were first equilibrated with the HL-60 cell culture media, and 2 μ l of HL-60 cells were added to one well to drive a flow of cells through the channels. Once the bulge was trapped with enough numbers of cells, the excess cells were rinse out by pipetting in two wells. The trapped cell number in the patterned bulges was counted after rinsing.

4.5.3 Image and data analysis

The two-photon images in Fig 4.8 were obtained as described in 2.5.6.

Chapter 5: CONCLUSION

5.1 Summary and Conclusion

The objective of this thesis is to further develop the technique of rapid 3-D laser microprinting by researching on the biological activity and functions of printed scaffolds and printed proteins. The rapid 3-D laser microprinting system was developed by Scott, and it includes a femtosecond laser setup for performing multi-photon photobleaching of biotin-4-fluorescein and fluorescein and a series of addition of chemicals for development of the printed microarchitectures and printed protein patterns. Using the technique, scientists and engineers are able to simultaneously generate 3-D defined microarchitecture of scaffolds and internal 3-D patterns of proteins inside scaffolds. The capability of this technique is promising in creating engineered tissue with high complexity for regenerative medicine and building in-vitro microenvironment for biology research. In order to further verify the properties and functions of the rapid 3-D laser microprinting system, in this thesis, we demonstrated several assays that assisted to prove the biological activity and functions of printed scaffolds and printed proteins, while revealed some potential applications of the technique.

The mechanism of leukocyte rolling has been thoroughly investigated for the leukocyte recruitment process occurring to the vascular wall induced by inflammation. Using the rapid 3-D laser microprinting technique, we created an in-vitro environment for presenting leukocyte rolling. This well-investigated rolling mechanism is suitable for verifying the printed proteins inside the printed scaffolds have the biological interaction with cells. After introducing HL-60 leukocytes into a microfluidic device containing printed collagen scaffolds and printed P-selectin patterns, the rolling occurred on the P-selectin patterned collagen channel due to the binding of PSGL-1 and P-selectin, while no rolling occurred on the unpatterned collagen channel. This result demonstrated that the rapid 3-D laser microprinting technique retains the biological activities and functions of printed protein cues, and it also suggested the potential application for drug screening assays in biomimetic environment.

Vascularization of engineered tissue has been demonstrated to accelerate the connection to the host vascular system after implantation, leading to an effective tissue repair. Using the rapid 3-D laser microprinting, a microvasculature inside collagen scaffolds could be easily created by seeding endothelial cells into the printed scaffolds with capillary-like geometries. Combining the leukocyte rolling assay with the printed microvasculature, HL-60 leukocytes were introduced into the printed microvasculature, which was activated by the printed internal patterns of IL-1 and LPS. HL-60 cell rolling occurred on the vascular wall inside the printed microvasculature. However, the rolling occurred on both IL-1 or LPS patterned and unpatterned collagen channels. This result suggested that the activated endothelial cells might express signals to their nearby cells, leading to the whole microvasculature activation. Nevertheless, the result still proved the biological activity and function were preserved by the printed protein cues. In addition, one potential application of the rapid 3-D laser microprinting might be the examination of a local effect of printed protein.

The rapid 3-D laser microprinting technique is promising in creating complex engineered tissue for regenerative medicine, such as stem cell niche. Many biologists and tissue engineers attempt to create artificial stem cell niche for exploiting its self-renewal and differentiation ability. We planed to create such engineered stem cell niche using our technique. We started from achieving the cell homing to specific locations inside scaffolds for creating the microenvironment of stem cell niches in the future. The HL-60 leukocyte rolling inspired the idea of printing the patterns of P-selectin for catching cell and directing cells into a trap. The cycle of innovation was conducted to achieve the goal of cell homing, thanks to the rapidly prototyping ability of the 3-D laser microprinting technique. Finally, the guiding and homing of cells was achieved, and it also verified that the combination of defined microarchitecture of scaffolds and patterns of proteins was necessary for this application.

In summary, the properties and functions of rapid 3-D laser microprinting has been further proved in this thesis, and we believe that this methodology of combined scaffold printing and patterning of internal protein cues could enable highly engineered therapeutic scaffolds for

regenerative medicine applications.

5.2 Potential Future Work

5.2.1 Improvement of leukocyte rolling assay in printed microvasculature

For the leukocyte rolling assay in printed microvasculature as described in *Chapter 3*, the evidence for the conclusions was still not convincing enough. To further investigate the leukocyte rolling in the activated printed microvasculature, more experiments should be implemented, and rolling assay should be conducted at different time point after seeding endothelial cells. Also, the control experiments should be designed more strictly, such as conducting rolling assay on the printed endothelium with patterned streptavidin only. Quantifying the results is also necessary for verifying the performance. The similar quantifying analysis as described in *Chapter 2* can be used, but in order to improve the quality of videos of rolling assay, we can simply increase the resolution of videos or stain the HL-60 leukocytes with dye or fluorescence. The improvement of leukocyte rolling assay in printed microvasculature provides rigorous results and the interaction within microvasculature could be further studied.

5.2.2 Next steps for creating engineered stem cell niche

In *Chapter 4*, guiding and homing of HL-60 cells was achieved inside printed microstructures of collagen scaffolds with internal patterned proteins. Next, we want to achieve guiding and homing of stem cells instead of HL-60 cells, and then introduce the endothelial cells to form microvasculature near the homed stem cells. As a result, a simple model of engineered stem cell niche can be created, since stem cell niche consists of stem cells, non-stem cells, blood vessels, and extracellular matrices with molecular signals.

The simple model of engineered stem cell niche can be created by performing several steps after printing of collagen scaffolds. First, we use mesenchymal stem cells (MSCs) and perform gene transfection to have them express PSGL-1, and the transfected MSCs can be flowed into printed collagen channels with printed P-selectin patterns (Fig 5.1a). After a quite amount of

MSCs are trapped and homed in the bulges, the device will be left overnight for MSC adhesion, proliferation and migration into the collagen scaffolds (Fig 5.1b). Last, endothelial cells can be flowed into the collagen channels to form the vasculature along the collagen channel walls, while passing by the bulges (i.e. without growing into the bulges) as shown in Fig 5.1c. As a result, the simple model of mesenchymal stem cell niche is created.

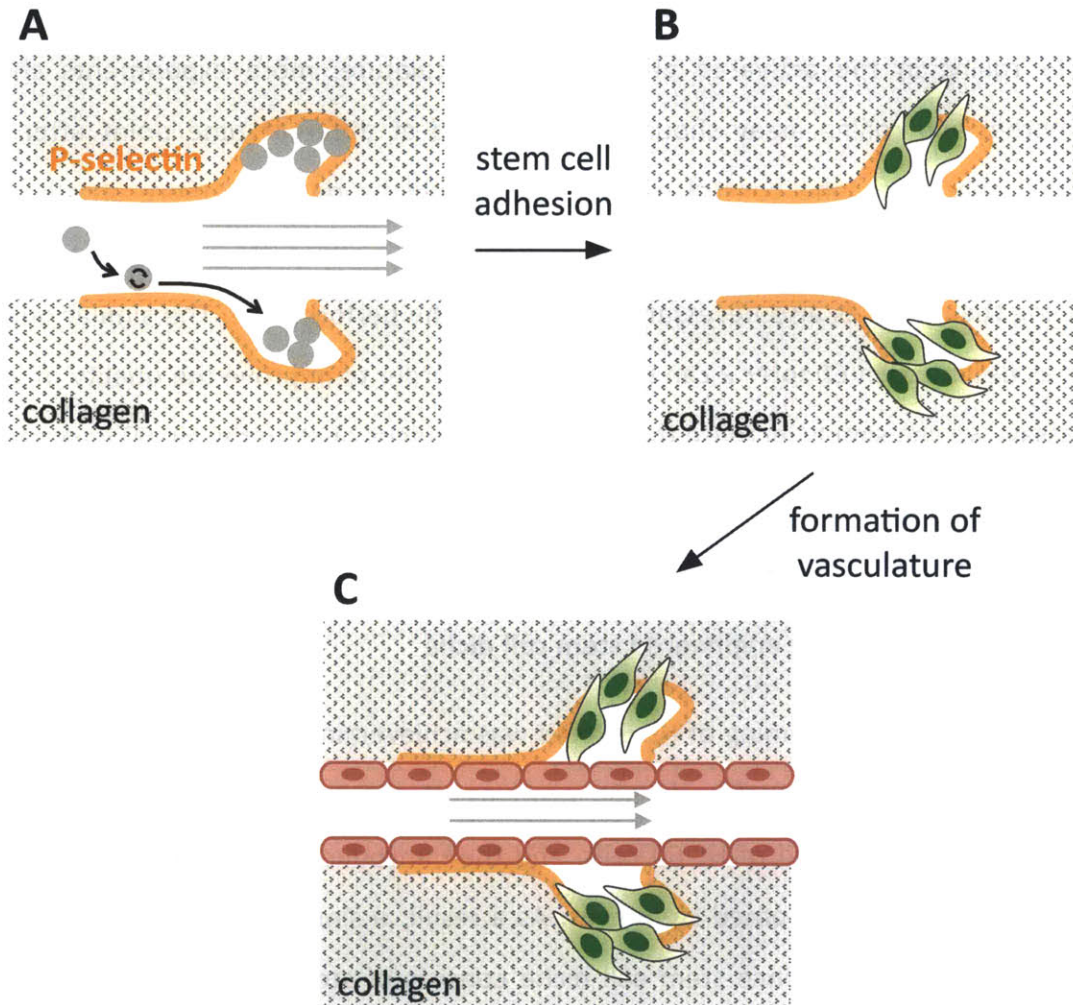


Fig 5.1: The simple model of engineered stem cell niche. (a) Transfected MSCs are flowed through the printed collagen channels, directed by P-selectin patterns and then trapped by the bulges. (b) The device is left overnight for MSC adhesion, proliferation and migration into the collagen scaffolds. (c) Endothelial cells are then flowed into the collagen channels to form microvasculature along the collagen channel.

Stem cell niche has high complexity in structures, functions and biological interactions. Achieving the simple model of engineered mesenchymal stem cell niche will determine the capability of creating more complex engineered stem cell niche in the future.

Reference

1. Scott, M. Ultra-rapid 2-D and 3-D laser microprinting of proteins. (2013). at <http://dspace.mit.edu/handle/1721.1/79248>
2. Berthiaume, F., Maguire, T. J. & Yarmush, M. L. Tissue engineering and regenerative medicine: history, progress, and challenges. *Annu. Rev. Chem. Biomol. Eng.* **2**, 403–30 (2011).
3. Copelan, E. a. Hematopoietic stem-cell transplantation. *N. Engl. J. Med.* **354**, 1813–26 (2006).
4. Langer, R. & Vacanti, J. P. Tissue Engineering. *Science* **260**, 920–925 (1993).
5. Gilbert, T. W., Sellaro, T. L. & Badylak, S. F. Decellularization of tissues and organs. *Biomaterials* **27**, 3675–83 (2006).
6. Sachlos, E. & Czernuszka, J. T. Making tissue engineering scaffolds work. Review: the application of solid freeform fabrication technology to the production of tissue engineering scaffolds. *Eur. Cell. Mater.* **5**, 29–39; discussion 39–40 (2003).
7. Engelmayr, G. C. *et al.* Accordion-like honeycombs for tissue engineering of cardiac anisotropy. *Nat. Mater.* **7**, 1003–10 (2008).
8. Miller, J. S. *et al.* Rapid casting of patterned vascular networks for perfusable engineered three-dimensional tissues. *Nat. Mater.* **11**, 768–74 (2012).
9. Yang, Y. *et al.* Fabrication and properties of a porous chitin/chitosan conduit for nerve regeneration. *Biotechnol. Lett.* **26**, 1793–7 (2004).
10. Koroleva, a *et al.* Two-photon polymerization-generated and micromolding-replicated 3D scaffolds for peripheral neural tissue engineering applications. *Biofabrication* **4**, 025005 (2012).

11. Phillips, J. B., Bunting, S. C. J., Hall, S. M. & Brown, R. a. Neural tissue engineering: a self-organizing collagen guidance conduit. *Tissue Eng.* **11**, 1611–7 (2005).
12. Hollister, S. J. Porous scaffold design for tissue engineering. *Nat. Mater.* **4**, 518–24 (2005).
13. Babensee, J. E., McIntire, L. V & Mikos, a G. Growth factor delivery for tissue engineering. *Pharm. Res.* **17**, 497–504 (2000).
14. Yoon, J. J., Song, S. H., Lee, D. S. & Park, T. G. Immobilization of cell adhesive RGD peptide onto the surface of highly porous biodegradable polymer scaffolds fabricated by a gas foaming/salt leaching method. *Biomaterials* **25**, 5613–20 (2004).
15. Hozumi, K. *et al.* Cell surface receptor-specific scaffold requirements for adhesion to laminin-derived peptide-chitosan membranes. *Biomaterials* **31**, 3237–43 (2010).
16. Chichkov, B. N. Two-Photon Polymerization: A New Approach to Micromachining. (2006).
17. Cumpston, B., Ananthavel, S. & Barlow, S. Two-photon polymerization initiators for three-dimensional optical data storage and microfabrication. *Nature* **398**, 51–54 (1999).
18. Kubes, P. Introduction: The complexities of leukocyte recruitment. *Semin. Immunol.* **14**, 65–72 (2002).
19. McIntyre, T. M., Prescott, S. M., Weyrich, A. S. & Zimmerman, G. a. Cell-cell interactions: leukocyte-endothelial interactions. *Curr. Opin. Hematol.* **10**, 150–8 (2003).
20. Kunkel, E. J. & Butcher, E. C. Plasma-cell homing. *Nat. Rev. Immunol.* **3**, 822–9 (2003).
21. Kubes, P. & Ward, P. a. Leukocyte recruitment and the acute inflammatory response. *Brain Pathol.* **10**, 127–35 (2000).
22. Kubes, P. & Kerfoot, S. M. Leukocyte recruitment in the microcirculation: the rolling paradigm revisited. *News Physiol. Sci.* **16**, 76–80 (2001).

23. Muller, W. How Endothelial Cells Regulate Transmigration of Leukocytes in the Inflammatory Response. *Am. J. Pathol.* (2014). at <<http://www.sciencedirect.com/science/article/pii/S0002944014000972>>
24. Rao, R. M., Yang, L., Garcia-Cardena, G. & Luscinskas, F. W. Endothelial-dependent mechanisms of leukocyte recruitment to the vascular wall. *Circ. Res.* **101**, 234–47 (2007).
25. Patel, K. D., Cuvelier, S. L. & Wiehler, S. Selectins: critical mediators of leukocyte recruitment. *Semin. Immunol.* **14**, 73–81 (2002).
26. Spertini, O., Cordey, a S., Monai, N., Giuffrè, L. & Schapira, M. P-selectin glycoprotein ligand 1 is a ligand for L-selectin on neutrophils, monocytes, and CD34+ hematopoietic progenitor cells. *J. Cell Biol.* **135**, 523–31 (1996).
27. Ley, K., Laudanna, C., Cybulsky, M. I. & Nourshargh, S. Getting to the site of inflammation: the leukocyte adhesion cascade updated. *Nat. Rev. Immunol.* **7**, 678–89 (2007).
28. Simon, S. I. & Green, C. E. Molecular mechanics and dynamics of leukocyte recruitment during inflammation. *Annu. Rev. Biomed. Eng.* **7**, 151–85 (2005).
29. Yilmaz, G. & Granger, D. N. Leukocyte recruitment and ischemic brain injury. *Neuromolecular Med.* **12**, 193–204 (2010).
30. Petri, B., Phillipson, M. & Kubes, P. The Physiology of Leukocyte Recruitment: An In Vivo Perspective. *J. Immunol.* **180**, 6439–6446 (2008).
31. Sundd, P., Pospieszalska, M. K., Cheung, L. S.-L., Konstantopoulos, K. & Ley, K. Biomechanics of leukocyte rolling. *Biorheology* **48**, 1–35 (2011).
32. Bianchi, E., Molteni, R., Pardi, R. & Dubini, G. Microfluidics for in vitro biomimetic shear stress-dependent leukocyte adhesion assays. *J. Biomech.* **46**, 276–83 (2013).
33. Lawrence, M. & Kansas, G. Threshold Levels of Fluid Shear Promote Leukocyte Adhesion through Selectins (CD62L,P,E). *J. cell ...* **136**, 717–727 (1997).

34. Dong, C. & Lei, X. X. Biomechanics of cell rolling: shear flow, cell-surface adhesion, and cell deformability. *J. Biomech.* **33**, 35–43 (2000).
35. Kim, M. & Sarelius, I. Role of shear forces and adhesion molecule distribution on P-selectin-mediated leukocyte rolling in postcapillary venules. *Am. J. Physiol. ...* **14642**, 2705–2711 (2004).
36. Laschke, M. W. *et al.* Angiogenesis in tissue engineering: breathing life into constructed tissue substitutes. *Tissue Eng.* **12**, 2093–104 (2006).
37. Kannan, R. Y., Salacinski, H. J., Sales, K., Butler, P. & Seifalian, A. M. The roles of tissue engineering and vascularisation in the development of micro-vascular networks: a review. *Biomaterials* **26**, 1857–75 (2005).
38. Novosel, E. C., Kleinhans, C. & Kluger, P. J. Vascularization is the key challenge in tissue engineering. *Adv. Drug Deliv. Rev.* **63**, 300–11 (2011).
39. Fidkowski, C. *et al.* Endothelialized microvasculature based on a biodegradable elastomer. *Tissue Eng.* **11**, 302–9 (2005).
40. Rouwkema, J., Rivron, N. C. & van Blitterswijk, C. a. Vascularization in tissue engineering. *Trends Biotechnol.* **26**, 434–41 (2008).
41. Kneser, U. & Polykandriotis, E. Engineering of Vascularized Transplantable Bone Tissues : Induction of Axial Vascularization in an Osteoconductive Matrix Using an Arteriovenous Loop. ... *Eng.* **12**, (2006).
42. Kneser, U. Tissue engineering of bone: the reconstructive surgeon's point of view. *J. Cell. ...* (2006). at
<<http://onlinelibrary.wiley.com/doi/10.1111/j.1582-4934.2006.tb00287.x/full>>
43. Tremblay, P.-L., Hudon, V., Berthod, F., Germain, L. & Auger, F. a. Inosculation of tissue-engineered capillaries with the host's vasculature in a reconstructed skin transplanted on mice. *Am. J. Transplant* **5**, 1002–10 (2005).

44. Levenberg, S. *et al.* Engineering vascularized skeletal muscle tissue. *Nat. Biotechnol.* **23**, 879–84 (2005).
45. Tedder, T., Steeber, D., Chen, A. & Engel, P. The selectins: vascular adhesion molecules. *FASEB J.* **9**, 866–873 (1995).
46. Kalebic, T., Garbisa, S., Glaser, B. & Liotta, L. a. Basement membrane collagen: degradation by migrating endothelial cells. *Science* **221**, 281–3 (1983).
47. Lutolf, M. P., Gilbert, P. M. & Blau, H. M. Designing materials to direct stem-cell fate. *Nature* **462**, 433–41 (2009).
48. Becerra, J., Santos-Ruiz, L., Andrades, J. a & Marí-Beffa, M. The stem cell niche should be a key issue for cell therapy in regenerative medicine. *Stem Cell Rev.* **7**, 248–55 (2011).
49. Scadden, D. T. The stem-cell niche as an entity of action. *Nature* **441**, 1075–9 (2006).
50. Vazin, T. & Schaffer, D. V. Engineering strategies to emulate the stem cell niche. *Trends Biotechnol.* **28**, 117–24 (2010).
51. Lutolf, M. P. & Blau, H. M. Artificial stem cell niches. *Adv. Mater.* **21**, 3255–68 (2009).
52. Kobel, S. & Lutolf, M. High-throughput methods to define complex stem cell niches. *Biotechniques* **48**, ix–xxii (2010).